2007

Development of a high average current polarized electron source with long cathode operational lifetime

C. K. Sinclair
Thomas Jefferson National Accelerator Facility, cks26@cornell.edu

P. Adderley
Thomas Jefferson National Accelerator Facility, adderley@jlab.org

B. M. Dunham
Thomas Jefferson National Accelerator Facility

J. C. Hansknecht
Thomas Jefferson National Accelerator Facility, hansknec@jlab.org

P. Hartmann
Thomas Jefferson National Accelerator Facility

See next page for additional authors

Development of a high average current polarized electron source with long cathode operational lifetime

C. K. Sinclair,[*,†] P. A. Adderley, B. M. Dunham,[*] J. C. Hansknecht, P. Hartmann,[‡] M. Poelker, J. S. Price,[§] P. M. Rutt,[‖] W. J. Schneider, and M. Steigerwald[¶]

Thomas Jefferson National Accelerator Facility, Newport News, Virginia 23606, USA

(Received 22 December 2006; published 7 February 2007)

Substantially more than half of the electromagnetic nuclear physics experiments conducted at the Continuous Electron Beam Accelerator Facility of the Thomas Jefferson National Accelerator Facility (Jefferson Laboratory) require highly polarized electron beams, often at high average current. Spin-polarized electrons are produced by photoemission from various GaAs-based semiconductor photocathodes, using circularly polarized laser light with photon energy slightly larger than the semiconductor band gap. The photocathodes are prepared by activation of the clean semiconductor surface to negative electron affinity using cesium and oxidation. Historically, in many laboratories worldwide, these photocathodes have had short operational lifetimes at high average current, and have often deteriorated fairly quickly in ultrahigh vacuum even without electron beam delivery. At Jefferson Lab, we have developed a polarized electron source in which the photocathodes degrade exceptionally slowly without electron emission, and in which ion back bombardment is the predominant mechanism limiting the operational lifetime of the cathodes during electron emission. We have reproducibly obtained cathode 1/e dark lifetimes over two years, and 1/e charge density and charge lifetimes during electron beam delivery of over 2×10^5 C/cm^2 and 200 C, respectively. This source is able to support uninterrupted high average current polarized beam delivery to three experimental halls simultaneously for many months at a time. Many of the techniques we report here are directly applicable to the development of GaAs photoemission electron guns to deliver high average current, high brightness unpolarized beams.

DOI: 10.1103/PhysRevSTAB.10.023501 PACS numbers: 29.27.Hj, 29.25.Bx, 41.75.Fr

I. INTRODUCTION

The Continuous Electron Beam Accelerator Facility (CEBAF) at Jefferson Laboratory was developed to conduct high-precision electromagnetic nuclear physics experiments at beam energies up to 4 GeV. The accelerator delivers high average current cw beams with small emittance ($\varepsilon_{n,\mathrm{rms}} < 1$ mm-mrad) and very low energy spread ($\Delta E/E_{\mathrm{rms}} < 2 \times 10^{-5}$). The accelerator is comprised of two nominally identical superconducting linear accelerators, and magnetic transport arcs that allow up to five recirculation passes through the linacs [1]. The performance of the superconducting accelerator cavities has been excellent, with the result that the accelerator now operates at energies approaching 6 GeV [2]. Using a third subharmonic rf chopping system in the injector and third subharmonic rf separators following each of the five recirculation passes, the accelerator can provide independent cw beam at various correlated energies to each of three experimental halls. The fundamental accelerator rf frequency is 1497 MHz, with every rf bucket filled in normal operation, so each experimental hall receives a 499 MHz cw bunch train. The accelerator can deliver up to 200 μA cw at full energy (limited by the installed rf power). Two of the three experimental halls are equipped to operate with up to 1 MW of beam power, while the third hall is used only with very low average beam current. The accelerator is operated for about 5000 hours per year, and routinely delivers high average current beam.

A substantial fraction of the CEBAF experimental physics program requires highly polarized electron beams. The source that delivers these beams must not only support the demanding beam quality specifications, but also provide high average current, highly polarized beam for extended periods of time. The fraction of the experimental program requiring polarized electrons is so large that in general at least one experimental hall requires polarized beam during all scheduled accelerator operation. This means that the polarized source necessarily delivers all beams, whether polarization is required or not, since the injector design requires that all electrons originate from the same cathode.

The beams delivered to the three experimental halls follow different paths after extraction from the accelerator, and are often derived from different numbers of recircula-

[*]Present Address: Wilson Laboratory, Cornell University, Ithaca, NY 14853.
[†]Corresponding author.
Electronic address: cks26@cornell.edu
[‡]Present address: Universitat Dortmund, Maria-Goppert-Mayer Str. 2, 44221 Dortmund, Germany.
[§]Present address: G.E. Healthcare, Niskayuna, NY.
[‖]Present address: SEAKR Engineering, 6221 S. Racine Circle, Centennial, CO 80111.
[¶]Present address: Carl Zeiss Lithos GmbH, D-73447 Oberkochen, Germany.

tion passes, so the total spin precession from the polarized source to each experimental hall is in general quite different. Since there is no net vertical bend between the injector and the experimental hall beam lines, and no energy difference between pairs of equal and opposite vertical bends, the net precession is entirely in the horizontal plane. When the precession angle difference between any two experimental halls is an integral multiple of π, the maximum longitudinal polarization from the injector can be delivered to both halls by properly orienting the polarization exiting the injector. There are approximately 400 two-hall energy combinations that give maximum polarization in two halls [3]. For occasions when all three halls require polarized beam, only two beam energies (2.1 and 4.2 GeV) can provide maximum longitudinal polarization to all three halls simultaneously; however, since a transverse polarization component is generally inconsequential to the physics experiments being conducted, this fact has allowed the simultaneous delivery of highly longitudinally polarized electrons to all three halls in a large number of cases. Finally, it is worth noting that there is negligible loss of polarization between the injector and the experimental halls [4].

The first polarized electron source for an accelerator, based on photoionization of state selected ^{6}Li atoms, was developed at Yale University for use at the Stanford Linear Accelerator [5]. Somewhat later, a polarized source based on the Fano effect in Rb was developed for the Bonn synchrotron [6]. Other polarized sources were developed or proposed during the 1970s, including an improved version of the Li photoionization source [7], a source based on the chemi-ionization of metastable He atoms [8], and sources using the Fano effect in Cs [9]. Despite some technical demonstrations, none of these latter sources were ever developed to the point of being operational accelerator injectors.

Following the 1974 demonstration of polarized electron photoemission from GaAs [10], polarized electron sources based on the use of GaAs photocathodes were developed and operated at a number of high energy and nuclear physics laboratories, including the Stanford Linear Accelerator Center [11,12], the Mainz Microtron [13,14], the MIT-Bates Laboratory [15], NIKHEF [16], and Bonn University [17]. The GaAs photocathodes of these sources were either prepared *in situ* in the electron gun, or in a separate chamber connected to the gun structure through a load-lock system. In each of these sources, the reported cathode dark lifetime—i.e. the 1/e lifetime of the cathode quantum efficiency without electron emission or cathode high voltage applied—ranged from some tens of hours to several hundred hours at best. Some of these sources observed very short cathode lifetimes with cathode high voltage applied, even with no photoemission current, leading to their operation below their original design voltage, or with low duty factor pulsed, as opposed to DC, applied cathode voltage. Most importantly, when operated with average beam currents of a few to several tens of microamperes, the cathode operational lifetimes were short, and varied roughly inversely with the average beam current. Total charges of no more than 5 to 20 C could be delivered from these sources before it became necessary to either clean and reactivate, or exchange, the photocathode.

None of the polarized sources described above could meet the demands of the planned experimental program at CEBAF. Accordingly, during a period of polarized source development, we sought to understand and reduce or eliminate the underlying causes of photocathode degradation during beam delivery, and to construct a source in which as large a fraction as possible of the electrons produced at the photocathode is transported to the experimental users. The final source we developed included unique lasers delivering cw trains of short-duration optical pulses stably locked to the accelerator rf frequency, and a prebuncher cavity to improve beam transmission through the injector chopping system. We incorporated both commercial nonevaporable getter (NEG) pumps and in-house prepared NEG films to provide excellent vacuum in the gun and its attached beam line. The elimination of electrons originating from the large-radius region of the photocathode was a very significant improvement. We eliminated all short focal length electron optical elements from the beam line. Atomic hydrogen cleaning was incorporated as part of the photocathode preparation process. The final injector has two nominally identical polarized electron guns. While the availability of two polarized guns provides a high degree of redundancy, it has proven possible to deliver high average current beam from a single gun for uninterrupted periods of months. At the present time, the predominant effect limiting the cathode operational life in these guns is ion back bombardment.

In the sections below, we summarize the evolution of the polarized injector through three different designs, with information on the operational experience with each. In parallel with the development of the polarized electron guns and beam lines, we summarize the development of several unique laser systems that greatly reduced the polarized beam losses through the injector chopping system, and provided considerable operational flexibility in delivering three simultaneous polarized beams. Following this summary of CEBAF polarized source and laser developments, noteworthy aspects of our ultrahigh vacuum techniques and photocathode preparation procedures are presented. Finally, we summarize the present performance of the polarized injector, and comment on the implication of our results for future polarized source developments. Negative electron-affinity photocathodes offer very small thermal emittances compared to other photocathodes [18], and much of the information presented here is relevant to the development of electron sources to deliver high average current, high brightness unpolarized beams.

II. THE FIRST CEBAF POLARIZED SOURCE

The first polarized source for CEBAF, shown in Fig. 1, was developed in collaboration with the University of Illinois. The design, construction, and characterization of this 100 kV DC source was the topic of the Ph.D. thesis of one of us (B. M. D.) [19]. This polarized gun was similar in many respects to the original SLAC polarized gun [11]. The gun was mounted with its beam axis vertical. The electron beam was deflected into the horizontal plane by an $n = 0, 72°$ sector dipole providing nominally equal focal lengths in each plane. Electron spin orientation was accomplished with a spin manipulator comprised of a pair of 107.7° double-focusing electrostatic bends and a total of eight solenoid lenses, as shown in Fig. 2. With longitudinal spin entering the spin manipulator, any spin orientation can be obtained at the exit by suitable settings of the eight solenoids. This configuration, known as the "Z" style spin manipulator, was originally proposed by Reichert [20] and first implemented by Engwall *et al.* [21].

Reproducible beam transport from the photocathode through the spin manipulator was exceptionally difficult to achieve—a fact that was not appreciated at the time the source was designed. The 12.8 mm diameter flat GaAs cathode was located in a Pierce electrode designed to focus a high current DC beam from the fully illuminated cathode to a small waist near the center of the anode aperture, only 70 mm from the cathode. In practice, however, the source was operated with a low average current beam by illuminating only a small spot on the cathode that was generally not on the electromagnetic axis of the gun. Both the sector dipole and the electrostatic bends had very short focal lengths, so the solenoid lenses in the system were necessarily operated with short focal lengths as well. The many short focal length elements resulted in beam trajectories that were very sensitive to small steering changes. The number of correction coils and view screens was very limited by the lack of space along the beam line, making it impossible to center the beam in each of the many focusing elements. Trajectories passing through the various focusing elements off axis experienced focusing errors from aberrations that were difficult to quantify or reproduce. The need to change solenoid settings in the spin manipulator to provide longitudinal polarization in the experimental halls at different accelerator energies, coupled with the difficulty in establishing beam transport through the injector, led to large amounts of time being required to set up each new beam polarization condition.

The photocathode illumination was originally provided by a cw Ti:sapphire laser pumped by an argon-ion laser, producing a continuous DC beam. The subharmonic chopper system in the injector was designed to pass a maximum pulse duration corresponding to 60° of fundamental frequency rf phase ($\sim$ 110 ps), to each of the three experimental halls. This system thus transmitted a maximum of one-sixth of the current from the source. The required DC current from the polarized gun was determined by the highest current required in any experimental hall. Variable slits in the chopper system reduced the currents to the other halls to the desired levels. Thus in practice the

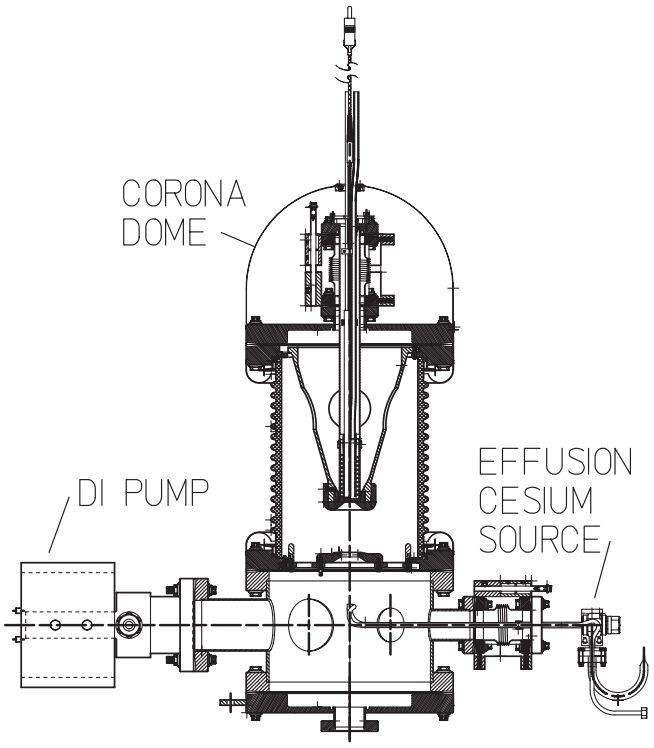

FIG. 1. The first CEBAF polarized electron source, developed in collaboration with the University of Illinois. The heater is shown inserted into the stalk cathode holder, and is removed during high-voltage operation.

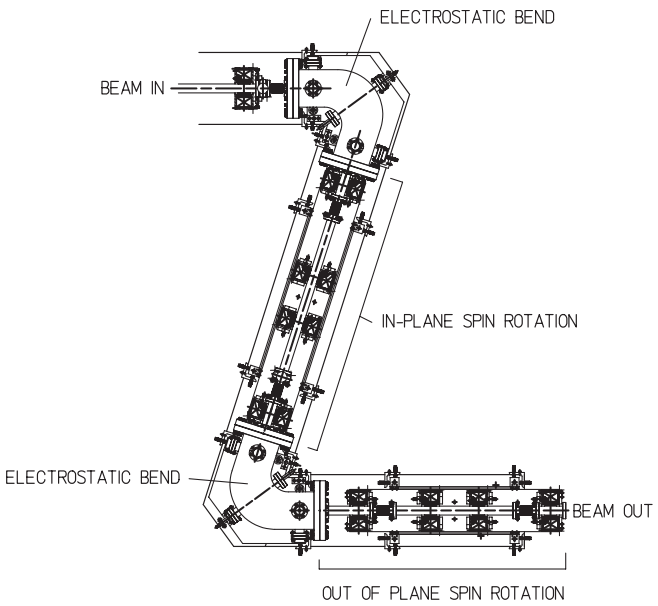

FIG. 2. The Z-style spin manipulator used with the first polarized electron source.

transmission through the chopper system was typically well below one-sixth. The loss of such a large fraction of the current from the polarized source was highly undesirable, particularly with the poor cathode operational lifetimes typical of the polarized sources at that time. Accordingly, we began development of lasers to produce continuous trains of suitably short-duration optical pulses synchronized with the fundamental accelerator rf frequency, to reduce beam losses through the chopper system.

This polarized source first provided beam to a single experimental hall from a bulk GaAs photocathode in February of 1997, using a master-oscillator power amplifier (MOPA) diode laser providing a 1497 MHz optical pulse train, described below. Average beam currents were typically 30 μA, with a maximum of 140 μA reached briefly. Polarized beam was first delivered to two experimental halls simultaneously during July and August of 1997. Measurements of the electron bunch length at the chopper slits, described below, showed that as the bunch charge increased, the electron bunch length increased to the point where there were significant losses at the chopper slits. Consequently, we installed a prebuncher cavity at a location about half-way between the gun and the chopper system. With the MOPA laser and this cavity, the beam transmission between the polarized gun cathode and the experimental halls was measured to be $\sim$70% at high average current. The beam losses were on the chopper slits, and in a two-aperture emittance filter located before the chopper. The average beam current was higher than in the earlier run, but the cathode operational lifetime was poor, requiring frequent interventions to reactivate or replace the cathode. It was observed that, as the average beam current was increased, the vacuum pressure in the gun increased dramatically. Thin-window Geiger tubes placed around the beam pipe between the gun and the 72° sector dipole, and between the exit of the sector dipole and the entrance to the spin manipulator, showed that the vacuum degradation was correlated with electron losses along this beam line.

Initially, the origin of this beam loss was puzzling, as the 12.8 mm diameter photocathode was illuminated close to its center with a Gaussian laser spot only $\sim$0.35 mm in diameter (FWHM). The beam spots observed on view screens downstream of the electron gun were small, symmetric, and well centered in the beam pipe, consistent with modeling, and showing that beam originating from the illuminated area of the cathode was far from all vacuum system walls. However, simulations showed that the trajectories of electrons originating from large-radius regions of the cathode, close to the junction between the flat cathode and the Pierce electrode, experienced transverse kicks sufficient to cause them to strike the beam pipe walls in the regions where the Geiger counters indicated beam losses. This situation was aggravated by the large number of short focal length electron optical elements.

As $\sim$30% of the laser light incident on the GaAs photocathode is reflected, it was speculated that subsequent reflection of this light from the uncoated laser entrance window might be the source of electrons originating from the large-radius regions. If this were the case, changing the entrance window for one that was antireflection coated would have reduced the beam losses by a factor of $\sim$10. On changing this window with a coated one, however, no change in the electron losses was observed, eliminating this possibility as the source of the problem.

Another possibility was that the large-radius electrons were being produced by photoemission generated by the recombination light emitted by the cathode itself. Electrons excited to the conduction band of the GaAs photocathode are either emitted, or, more likely, recombine. On recombination, they emit near band gap photons. These photons may reflect or scatter from the cathode surface, or from the many metal surfaces in the gun, and thus reach the large-radius regions of the photocathode after multiple reflections or scatterings. Absorption of these near band gap photons, though small, can lead to subsequent photoemission at large radius.

To test this hypothesis, a photocathode with negligible quantum efficiency at large radius was prepared by cleaning, prior to activation, only the central region of the GaAs cathode wafer. This produced a cathode with high quantum efficiency only in the cleaned area. The first beam test with this cathode was dramatic. Average beam currents of several hundred microamperes produced essentially no detectable vacuum pressure rise in the gun or Geiger counter activity along the beam line, and several coulombs of charge were quickly delivered with only a very slight reduction of the quantum efficiency. The elimination of electrons originating from large-radius areas of the photocathode has had a major beneficial impact on polarized electron delivery for the CEBAF accelerator, and has since been incorporated into other photoemission electron guns for both polarized and unpolarized beam delivery [22].

III. THE SECOND POLARIZED INJECTOR

At the time of the above test, construction of a new polarized electron gun and spin manipulator was well underway. This new source was designed to eliminate or reduce the impact of the shortcomings identified during operation of the original source at high average current. We removed the majority of the short focal length elements by replacing the Z spin manipulator with a Wien filter plus solenoid. The angle of the Pierce cathode electrode was significantly reduced. Massive nonevaporable pumping was added in the gun to provide improved vacuum. The new gun design incorporating this pumping is shown in Fig. 3. The 1497 MHz MOPA laser was exchanged for a set of three 499 MHz MOPA lasers, giving an independent laser for each experimental hall. Taking advantage of the rf time structure on the beam, we added beam position monitors, to improve the reproducibility and reduce the setup time of the injector optics. Finally, we developed a process

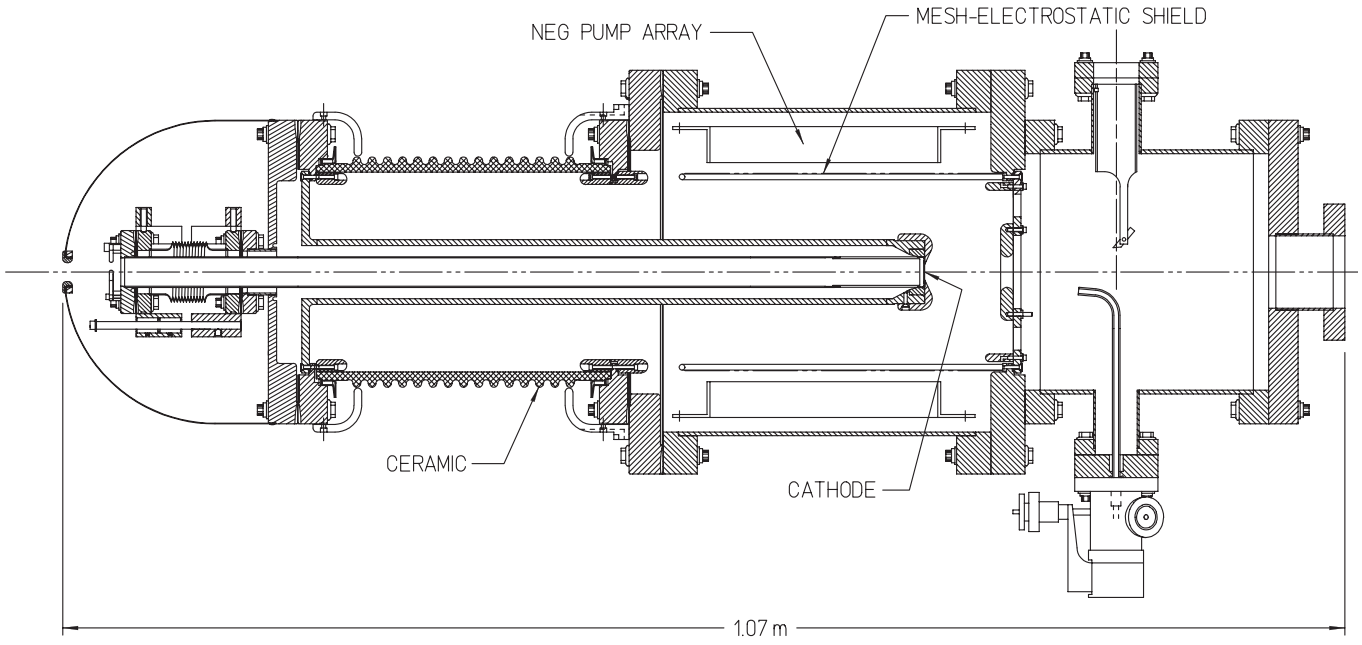

FIG. 3. The second polarized electron source, originally oriented in the vertical plane and later in the horizontal plane. Nonevaporable getter modules surround the cathode/anode gap. Other improvements are described in the text.

to reliably make photocathodes with no quantum efficiency at large radius. These changes are described below.

The Pierce electrode angle was changed from 39° to 25°, greatly reducing the focusing at the cathode. The replacement of the Z spin manipulator with a combination of a Wien filter and a solenoid eliminated both electrostatic bends and many solenoids. A Wien filter is a device with static electric and magnetic fields perpendicular to each other and to the velocity of charged particles passing through it, as shown in Fig. 4. Unit charged particles with a velocity of $\beta c = E/B$ are undeflected in passing through the Wien filter, while the spin is rotated in the plane of the electric field.

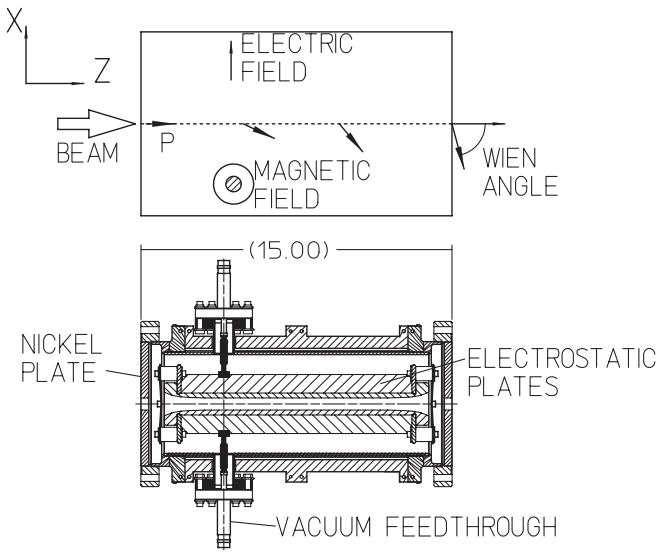

FIG. 4. The Wien filter spin manipulator used with CEBAF's second and third polarized electron sources. The magnet is not shown in the cutaway view.

Our Wien filter design was scaled from the SLAC design used on their original 66 keV GaAs polarized source to our 100 keV energy. A window-frame dipole magnet provided the magnetic field. The magnet was terminated at each end with a nickel plate having a 20 mm diameter beam aperture. The full magnet, assembled on the Wien filter vacuum chamber, was carefully mapped with a precision Hall probe. The profile of the electric field plates was calculated, using the code POISSON [23], to produce an electric field profile closely matching the magnetic field profile. Since the beam lines through the injector and in each experimental hall are purely horizontal, the Wien filter had a horizontal electric field. The Wien filter was capable of ±110° spin rotation at 100 keV. The calibration and performance of this Wien filter is described in Grames *et al.* [24].

All solenoids following the Wien filter were "counterwound"—i.e., they had two identical coils separated by a soft steel yoke, wired to produce equal and opposite longitudinal fields. These solenoids thus focused the beam without rotating any transverse polarization component. Two of these lenses had separate power supplies for each coil, allowing any small net spin rotation out of the horizontal plane to be compensated while maintaining the correct focusing.

The elimination of the Z spin manipulator substantially reduced the distance between the photocathode and the chopping apertures, reducing the bunch lengthening due to space charge [compare Figs. 5(a) and 5(b)]. The pre-

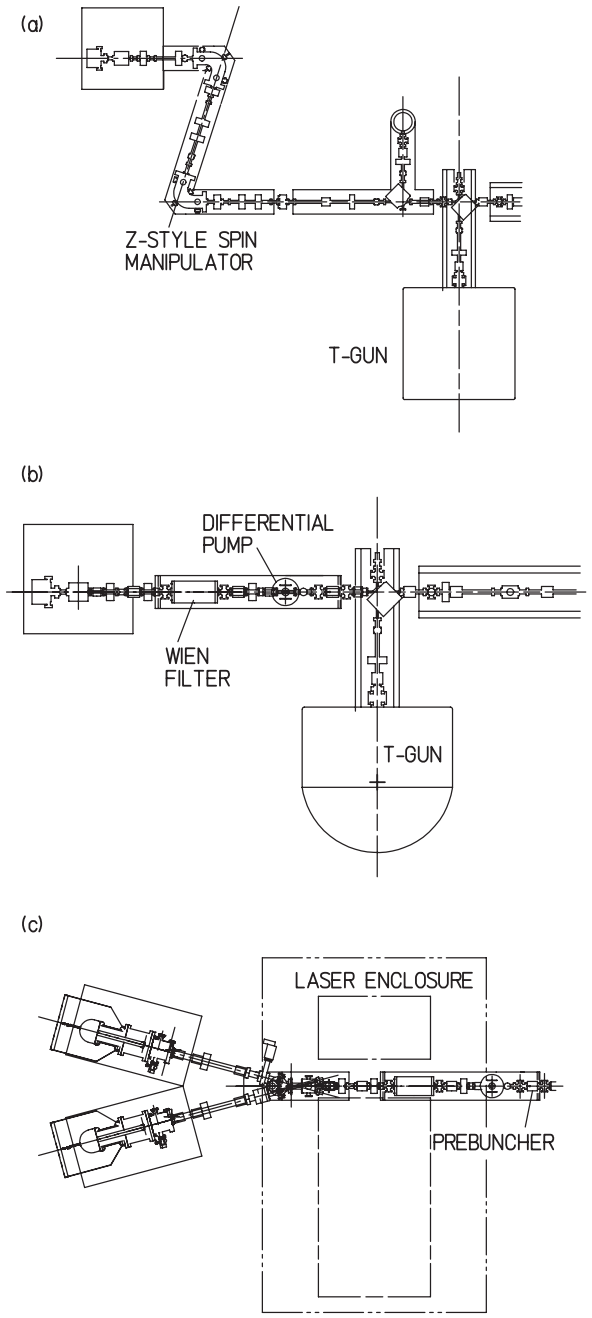

FIG. 5. The three CEBAF photoinjector designs. The photoguns used for the first and second polarized injectors extend out of the plane of (a) and (b) and are not shown. Today's photoinjector, (c), is so reliable the thermionic gun (T-gun) has been removed.

buncher cavity was retained, and located near the midpoint between the gun and the chopping system.

The vacuum in the vicinity of the photocathode was improved by the addition of an array of ten commercial NEG pumps surrounding the cathode-anode gap, as shown in Fig. 3 [25]. The NEG pumps, when activated to the manufacturer's specifications, provided a pumping speed of ~ 4 m^3/s for H_2, and ~ 2.2 m^3/s for CO. After an initial activation, these pumps were reactivated only by the ~ 30 h, 250 °C gun bakeout following cathode installation.

Since using an rf gain-switched laser produced a beam with rf time structure throughout the injector, standard rf beam position monitors (BPMs) could be employed. As space along the beam line was at a premium, a minor redesign of the standard CEBAF BPM was done, shortening its length and slightly reducing its diameter. The diameter reduction allowed us to mount commercial air-core dipole correction magnets directly on the BPM body [26]. The BPM signals were very similar to those in the accelerator, and standard electronics were used for readout [27]. The injector BPMs allowed us to develop scripts to automate resteering the beam after a Wien filter change or a relocation of the illuminated spot on the photocathode.

We replaced the single 1497 MHz MOPA laser with three 499 MHz MOPA lasers, providing independent control of the beam current to each hall. With the current controlled by the laser intensity, rather than the associated chopper slit, the overall transmission between the photocathode and the experimental halls was further improved. Beams from the three lasers were combined to illuminate a common point on the photocathode by using orthogonal linear polarization of the beams for the two high intensity halls, and either a dichroic or partially transmissive mirror for the low intensity beam. All beams passed through a single Pockels cell, which controlled the polarization for all halls. Software feedback loops and independent computer controlled optical attenuators for each laser maintained the beam current constant in each hall. These attenuators could also be programmed to give a ''soft-start'' current ramp for experiments using sensitive target cells.

To reliably eliminate photoemission from the large-radius areas of the photocathode, we did not want to rely on limiting the cathode area that was cleaned, or on masking the cathode area to which cesium was applied during activation. Instead, we developed a method, described below, to anodize an annular region on the cathode wafer. This anodized area, about 100 nm thick, does not support photoemission even when exposed to large quantities of cesium from multiple cathode activations.

Beam delivery from the redesigned polarized injector began in February of 1998, and was immediately successful. Several high average current polarized beam experiments were supported by this source soon after its installation. Perhaps most importantly, the first phase of an experiment to measure parity violation in electron scattering was completed [28]. This experiment placed very demanding requirements on the allowable level of helicity correlated systematic changes in beam position and energy at the experimental target. The polarized source and the full accelerator provided beam significantly better than the experimental requirements. This was the first time that a demanding parity-violation measurement was conducted

so early in the life of an accelerator, and the first time that an accelerator delivered beam to other experimental halls while simultaneously conducting a parity-violation measurement. A bulk GaAs photocathode was used for this parity-violation experiment. Following that experiment, we installed a thin, unstrained GaAs cathode to obtain a somewhat higher beam polarization for another high average current experiment. After completing the scheduled high average current operation in August of 1998, we installed a thin, strained GaAs cathode to produce much higher polarization. Until recently, all subsequent beam delivery was from these strained cathodes, which were grown to the SLAC specification [29]. Since May of 2004, we have used strained GaAs-GaAsP superlattice material, which provides both higher polarization and higher quantum efficiency (typically about 85% polarization and 0.5% quantum efficiency) [30].

IV. THE THIRD POLARIZED INJECTOR

Even as the second polarized source was being installed, it was recognized that the few remaining short focal length elements should be removed, and that further vacuum system improvements could be made in the course of removing these elements. Removal of these last short focal length elements eliminated the possibility of bending the beam from vertical to horizontal, requiring the polarized gun to be mounted in the horizontal plane. With a horizontal gun mounting, it is necessary to have the gun at an angle to the injector axis, or to locate an optical mirror internal to the vacuum system and close to the beam axis, to provide for illumination of the photocathode. As the internal mirror complicates the delivery of circularly polarized light to the cathode, and may be damaged by beam loss, it was decided to mount the polarized gun at 15° to the injector axis. For operational redundancy, two nominally identical guns were constructed, each identical to the upgraded vertical gun shown in Fig. 3, and mounted at equal and opposite 15° angles to the main injector axis, as shown in Fig. 5(c).

The 15° bending magnet that deflected the beam from either of the guns onto the injector axis was an air-core dipole made of four saddle-shaped coils. This magnet was designed to have a very long focal length—about 3 meters—and to be very close to anastigmatic. Magnetic measurements on the finished coil indicated that these goals were achieved [31]. Optical tables on either side of the beam line downstream of the 15° dipole and an arrangement of mirrors, including one remotely inserted, delivered linearly polarized light from the laser system to either gun. Pockels cells at the optical entrance windows to each gun then generated circular polarization. Switching beam delivery between the two guns was a fairly quick process, requiring about an hour. This time was required to switch high-voltage cables to the guns, and to verify the beam orbit through the injector.

A further vacuum improvement was made by enlarging the diameter of the beam tube between each polarized gun and the 15° bend magnet chamber, and depositing a nonevaporable getter film on the inner wall of these beam tubes [32]. Initially, a Ti-Zr film was used, followed more recently by a Ti-Zr-V film. These nonevaporable getter films offer several advantages in addition to their high pumping speed for chemically active gases. They form a diffusion barrier for gases diffusing from the wall of the beam tube. They have a lower thermal outgassing rate than the metals used for beam tubes [33]. The long beam tube with an active pumping surface offers an excellent geometry for pumping gases originating from further downstream in the injector. Finally, measurements have shown that electron stimulated desorption from nonevaporable getter films is lower than for typical metal surfaces by factors of 10 to 30 [34].

This third implementation of the polarized electron source, with two horizontal electron guns, has been in continuous use since its installation in July of 1999. At the time of this installation, we had sufficient confidence in the performance of the polarized gun to remove the origi-

TABLE I. Key features of each CEBAF photoinjector, with explanation for each value described within the text. Lifetime values for the first and second photoinjectors were not determined with great accuracy and represent estimates.

	First photoinjector	Second photoinjector	Third photoinjector
Date	Feb. 1995–Jan. 1998	Feb. 1998–June 1999	July 1999 to present
Gun orientation	Vertical	Vertical	Horizontal
Spin manipulator	Z style	Wien filter	Wien filter
Distance to chopper (m)	11	7	7
Number of short focal length elements	11	3	0
Pump speed (for hydrogen)	$\sim$0.5 m^3/s	$\sim$4 m^3/s	$\sim$4 m^3/s plus NEG-coated beam line
Portion of photocathode activated to NEA	100%	15%	15%
Dark lifetime (h)	$<$1000	Not measured	$>$22 000
Charge lifetime (C)	$<$10	$\sim$100	200
Charge density lifetime (C/cm^2)	$\sim 10^4$	$\sim 10^5$	2×10^5
Polarization	$\sim$35%	70%–75%	$>$80%

nal thermionic gun, which had been retained as a backup source. The maximum beam delivery from one polarized gun has exceeded 17.5 C in one day, corresponding to a current of over 200 μA averaged over 24 hours. Over 8000 C have been extracted from high-polarization photocathodes in these guns from their initial installation to the present. No other polarized electron source has approached this level of polarized beam delivery. Table I summarizes key features of each CEBAF photoinjector.

V. LASER DEVELOPMENT

It was clear at the beginning of our polarized source development that a very large gain was to be had by reducing or eliminating the losses in the chopper system. Doing so required one or more lasers producing trains of short duration near infrared optical pulses at either 499 or 1497 MHz. Commercial laser systems with these characteristics were unavailable at that time. Accordingly, we began a laser development program to meet our specific requirements.

While it was known that diode lasers could be gain switched at GHz frequencies, the optical output power of such lasers was far too low to support delivery of the required beam current. We developed a diode laser master oscillator—power amplifier (MOPA) configuration to greatly increase the available optical power [35]. In this scheme, shown in Fig. 6, the output of an rf gain-switched diode laser oscillator, the seed laser, was focused into and amplified by a tapered-stripe traveling-wave diode laser amplifier. The temperatures of both the seed and the amplifier diodes were maintained constant with thermoelectric coolers. An optical isolator prevented retroreflected light and spontaneous emission from the amplifier from entering the seed laser, where it could cause instabilities. The entire laser was built on an Invar plate with three tooling balls for mounting. The tooling balls rested in a conical hole, a groove, and on a flat plate, allowing the laser to be easily removed and replaced with high precision.

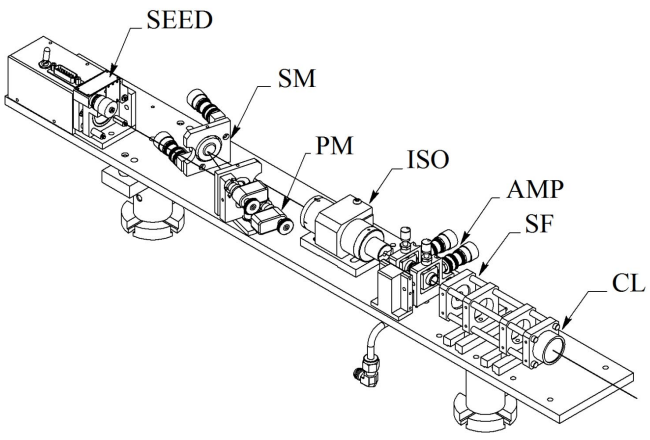

FIG. 6. The MOPA gain-switched diode seed laser and diode amplifier system: SM, steering mirror; PM, picomotor; ISO, optical isolator; AMP, single pass diode amplifier; SF, spatial filter; CL, cylindrical lens.

The optical output of the amplifier is composed of amplified seed laser light and a quasi-DC background from amplified spontaneous emission (ASE). Much of the ASE is removed in a 75 μm wide single axis spatial filter. The beam from the amplifier is quite asymmetric, requiring a cylindrical lens to create a nearly symmetric beam. The resulting beam is nearly diffraction limited, allowing a tight focus at the photocathode. Focused spots as small as $\sim$350 μm FWHM were obtained at the cathode, nearly 2 m from the focusing lens. This laser delivered average optical output powers approaching 100 mW over the wavelength range of $\sim$780 to 850 nm, at repetition rates of 499 or 1497 MHz. The width of the laser pulses was typically 60 to 80 ps FWHM, well below the pulse duration passed by the chopper system. The wavelength and output power of these MOPA lasers was ample for beam delivery from a polarized source using bulk GaAs photocathodes.

These MOPA lasers proved to be compact, reliable, and turn-key, requiring very little maintenance. As the seed laser is driven by rf power derived directly from the accelerator rf, synchronization and phase stability are automatically obtained without feedback loops. Low-frequency modulation of the diode amplifier current provides a simple means of producing low duty factor pulsed beams suitable for accelerator tune up. However, these lasers also have their drawbacks. Their wavelength is limited to specific values determined by the products offered by commercial diode laser manufacturers. Seed and amplifier diodes can presently be purchased at 770, 810, 830, and 850 nm. The seed diode may be temperature tuned by about $\pm$3 nm, but this range is too small to be very useful. Long-term diode availability is a concern.

We ultimately built a system of three 499 MHz lasers, providing an independent laser for each experimental hall. The ASE, about 2% of the total output power of each laser, poses a problem in three-laser operation, however. ASE from each laser generates beam in all experimental halls, reducing the average polarization in each hall. The ASE fraction increases significantly as the total power of a laser is increased by increasing the current to the amplifier diode. Thus, the total useful power available from one of these lasers is a tradeoff between increased output and increased ASE. We ultimately operated the 499 MHz lasers at about 70 mW average output power, while the 1497 MHz lasers could deliver $\sim$150 mW. In practice, with the transmission losses from the many optical components following the laser, one 499 MHz MOPA could deliver an average current of about 50 μA for extended periods of time from a thin photocathode providing high polarization. The low average power from these MOPA lasers is their most significant limitation.

Using a MOPA laser and the injector chopper system, we studied the temporal shape of the electron bunches at the location of the chopping slits as a function of the bunch charge. The chopping system uses a pair of 499 MHz TM_{210} mode rf deflecting cavities [36]. Each cavity was driven in two (degenerate) orthogonal transverse deflecting modes, phased to sweep the beam in a circle with a revolution frequency of 499 MHz. Six tuners on each cavity assured that the fields of the two deflecting modes were orthogonal and resonant at 499 MHz. Beam at the center of the first cavity was imaged to the center of the second cavity by a pair of counterwound solenoid lenses immediately before and after the chopping apertures, located midway between the two cavities. The amplitudes and phases of the fields in the second cavity were set to completely remove the rf kick from the first cavity. The chopping aperture system transmitted a maximum beam pulse duration equivalent to 60° of fundamental frequency rf phase (20° at 499 MHz) through each of three azimuthally separated paths. The transmission of each channel was smoothly variable from zero to maximum by a movable slit. Thus, the chopping system produced, at its exit, a 1497 MHz pulse train comprised of three interleaved 499 MHz pulse trains, with the charge per bunch in each train determined by the variable opening of its particular chopping slit.

For the temporal profile studies, two chopping apertures were completely closed, and the third set to transmit only a short-duration slice of the full electron bunch. By varying the phase of the rf drive to the laser with respect to the phase of the rf drive to the chopper cavities, and measuring the beam current transmitted through the narrow chopper aperture with a downstream Faraday cup, we measured the temporal profile of the bunch at the chopper slit. A series of chopper slit scans are presented in Fig. 7, showing the bunch lengthening and distortion with increasing bunch charge due to space charge acting over the ~11 m distance between the electron gun and the chopper slits. These bunch length measurements led us to add a fundamental frequency prebuncher cavity approximately midway between the polarized electron gun and the chopper slits, to improve beam transmission through the chopper system at higher average current [37].

The temporal response of GaAs photocathodes is of some interest. Two measurements have been reported. The first showed that illumination with a short-duration green optical pulse produced an electron bunch no longer than about 40 ps [38]. The second, with much better temporal resolution, demonstrated that illuminating the cathode with a very short-duration optical pulse of near band gap wavelength gives a ~20 ps temporal response for the electron emission, independent of the cathode quantum efficiency [39]. For our measurements, the width of the optical illumination pulse was determined by autocorrelation to be ~52 ps FWHM (with an assumed Gaussian

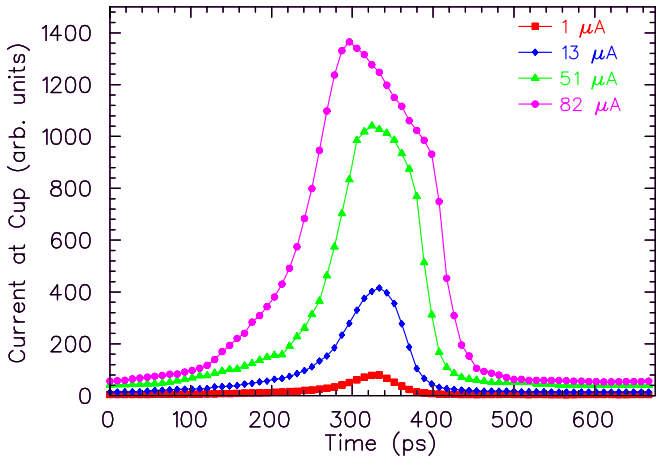

FIG. 7. (Color) Electron bunch length plots at the chopper slits at four different beam currents, obtained from a bulk GaAs cathode in the first polarized electron source. The observed bunch lengthening at higher current led to the installation of a 1497 MHz prebuncher between the gun and the injector chopper.

temporal profile) [40]. Figure 8 shows our autocorrelation optical pulse profile and the measured electron bunch profile. With our long duration optical pulse, our temporal resolution is not competitive with that reported in Ref. [39], and we have not done a fit to the measured bunch profile incorporating the effects of beam size at the chopper slit. However, our results are consistent with the temporal response reported in Ref. [39].

Mode-locked Ti:sapphire lasers offer considerably higher power than the MOPA diode lasers, but commercial systems delivering picosecond pulses and pulse repetition rates above ~120 MHz were not available at the time of our work. We developed a harmonically mode-locked Ti:sapphire laser to overcome the power limitations of

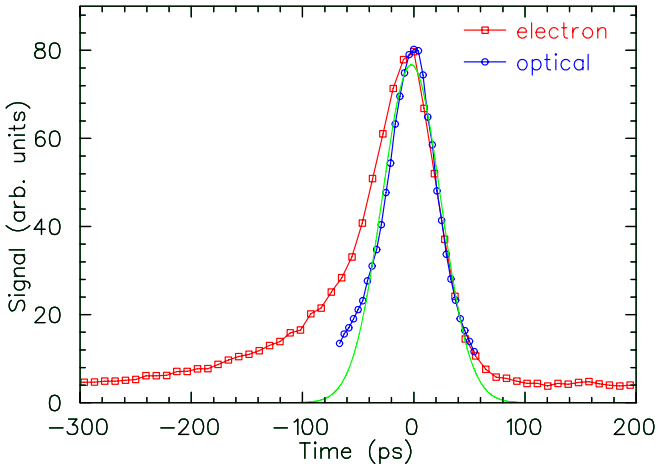

FIG. 8. (Color) Comparison of the optical pulse width and the electron bunch length at low current. The green curve is a 52 ps FWHM Gaussian fit to the optical pulse as measured by autocorrelation.

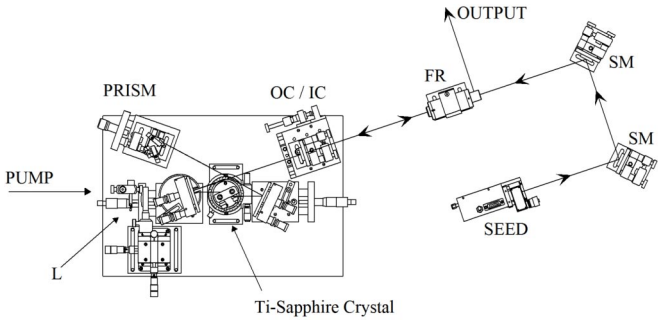

FIG. 9. The harmonic mode-locked Ti-sapphire laser: L, lens; OC/IC, output/input coupler; FR, Faraday rotator; SM, steering mirror; SEED, gain-switched diode seed laser. The Ti-sapphire laser emits rf-pulsed light (exiting after the Faraday rotator) when the seed laser pulse repetition rate is set to a multiple of the Ti-sapphire laser cavity free spectral range.

the MOPA lasers [41]. Mode locking was obtained by introducing light from a gain-switched diode laser into the Ti:sapphire laser cavity, as shown in Fig. 9. Mode-locked operation occurs when the time between pulses of the gain-switched diode is a harmonic of the optical round trip transit time of the Ti:sapphire cavity. We obtained repetition rates from 250 MHz to 3 GHz (in multiples of 250 MHz) from a laser with a cavity length of ~60 cm (fundamental frequency ~250 MHz). We believe the mode-locking mechanism is modulation of the Ti:sapphire gain at the cavity axial mode spacing by the introduced diode laser pulses.

The mode-locked Ti:sapphire laser uses a double-fold cavity design. The Ti:sapphire crystal (20 mm long by 6 mm diameter with Brewster angle faces, 0.03% dopant) is mounted in a water cooled copper block midway between two 10 cm radius of curvature mirrors. The double-fold cavity corrects for the astigmatism introduced by the Brewster cut crystal faces. Operation at either 780 or 860 nm could be obtained by exchanging cavity mirrors and the gain-switched diode wavelength. At each wavelength, the laser could be tuned over ~20 nm by adjusting the orientation of an intracavity prism near the high reflector. Light exits the laser through a ~95% reflectivity output coupler mirror, which also serves as the input coupler for the gain-switched diode beam. The input and output beams are separated by a Faraday rotator, a half-wave plate, and a polarizing cube. The gain-switched diode light passes through these components with no polarization rotation, while the Ti:sapphire laser beam is rotated 90° and reflected out of the polarizing cube. This laser produces ~50 ps duration pulses and over 500 mW output power when pumped with 5 W of green light from a solid-state frequency-doubled Nd:YVO_4 laser. The output power is independent of the laser repetition rate.

The Ti:sapphire laser is far more complex than the diode MOPA laser, and requires more maintenance. Its maximum output power fell by a factor of 2 over about three weeks due to dust accumulation on the mirrors. The output power was fully restored by cleaning the mirrors, which unfortunately required a realignment of the laser. A nitrogen purged box surrounding the laser cavity helped to reduce the dust problem, and remotely controlled mirror mounts were used to allow optimization of the output power and stability without interruption of accelerator operations. This laser showed significantly higher amplitude noise compared to the diode MOPA lasers. This is very likely because we did not actively stabilize the laser cavity length. Although we mounted the output coupler on a piezo-driven translation stage to provide a means for cavity length stabilization, an effective feedback loop was not implemented. We have demonstrated higher output power from this laser with higher pump power, and we believe that future high average current polarized sources might benefit from further development of the harmonically mode-locked Ti:sapphire laser. Table II compares the key features of the diode MOPA and mode-locked Ti:sapphire laser systems used at CEBAF.

Laser setups were chosen to match the experimental program. A mix of the Ti:sapphire laser and the diode MOPAs was selected to most efficiently deliver the required average currents to the three halls. A typical laser setup is shown in Fig. 10. In this particular setup, a diode

TABLE II. A comparison of features for the diode MOPA and mode-locked Ti:sapphire drive lasers developed for CEBAF.

	Diode MOPA	Ti-sapphire
Pulse-forming mechanism	Gain switching	Harmonic mode-locking
Repetition rate	0.1 to 3 GHz, continuous	0.1 to 3 GHz, discrete
Pulse width	~50 ps	~50 ps
Wavelength range	780, 810, 840 nm	Tunable over 30 nm range between 750 and 870 nm, depending on mirror set
Maximum power	70 mW at 499 MHz, 150 mW at 1497 MHz	500 mW
Maintenance required?	No	Weekly

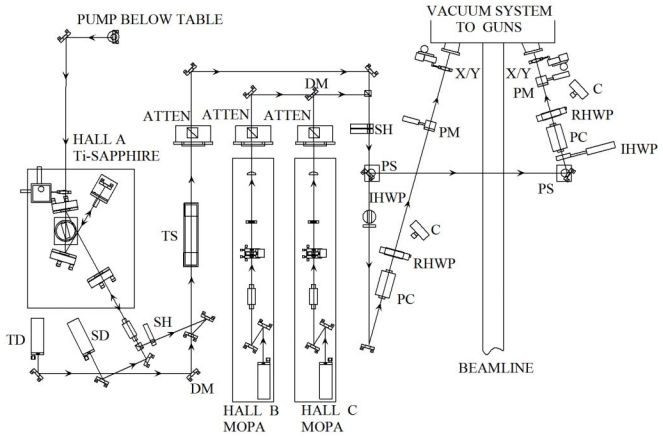

FIG. 10. A typical laser system configuration. The harmonic-mode-locked Ti-sapphire laser provides high current, high-polarization beam to one experimental hall. MOPA lasers provide low current, high polarization, and high current unpolarized beams to the other two halls. Numerous optical components, many remotely controlled, are required for routine operation and are described in the text: T, tune-mode diode laser; SD, gain-switched diode seed laser; SH, shutter; DM, dichroic mirror; TS, telescope; IHWP, insertable half-wave plate; PC, Pockels cell; C, camera; ATTEN, laser attenuator; PM, power meter; RHWP, rotating half-wave plate; X/Y, focusing lens mounted to translation stages; PS, periscope mirrors.

MOPA at 770 nm provides high average current, low polarization beam to one hall, a second diode MOPA at 850 nm provides low current, high-polarization beam to the low current hall, and the Ti:sapphire laser at 850 nm provides high current and high polarization to the second high average current hall.

A large number of optical components, many remotely controlled, are located between the lasers and the entrance window to the electron gun vacuum system. Beams from the three lasers are combined to be on a single axis by a combination of beam splitters, polarizers, and dichroic mirrors. Mirror mounts with picomotor adjustment screws allow precise alignment of the illuminated spot from each laser on the photocathode. Attenuators comprised of fixed linear polarizers and stepper motor controlled half-wave plates are in each laser beam line. A Pockels cell on the common optical beam line, operated at quarter-wave voltage, creates circular polarization. The polarization is reversed at a rate and in a pattern determined by the experiment, to aid in understanding and eliminating the systematic asymmetries in the electron beam properties (e.g. intensity, position) associated with polarization reversal. An insertable high quality mica half-wave plate is used to reverse the sense of the circular polarization produced by a particular sign of the Pockels cell voltage. A second Pockels cell operated at low voltage provides a small intensity modulation for those experiments, such as parity-violation measurements, that demand a very small correlation between bunch charge and polarization. Finally, a focusing lens near the entrance window to the gun sets the beam size at the photocathode. This lens is mounted on two orthogonal stepper motor controlled translation stages to move the laser spot on the cathode. This is useful both for mapping the quantum efficiency of the photocathode, and for delivering beam from different locations on the cathode. While the MOPA lasers could be used to generate a low duty factor beam tuning mode by modulating the current drive to the diode amplifier, the Ti:sapphire laser required a separate optical system to accomplish this. This system employed a fixed linear polarizer, an insertable half-wave plate, and a Pockels cell operated at half-wave voltage. The use of two laser types and this optical system provides a highly flexible way to match the electron beam from the photoemission gun to the needs of the three experimental halls.

VI. VACUUM SYSTEM PRACTICES AND PERFORMANCE

All of the photoemission guns and beam lines described above were carefully assembled to ultrahigh vacuum standards. Fabricated components were cooled with sulfur and silicone free lubricants during machining. All components were ultrasonically cleaned in an alkaline cleaner and deionized water solution at high temperature, followed by hot and cold deionized water rinses, an acetone rinse, and air drying. Internal components were assembled with vented, silver-plated stainless steel screws. All flanges have standard knife-edge seals. Copper gaskets are silver plated over an electroless nickel-plated diffusion barrier. Flanges are sealed using silver-plated high strength stainless steel bolts and stainless steel nuts. Bellville washers are used on most flanges larger than 70 mm, to assure reliable sealing during the expansion and contraction cycles of high temperature bakeouts.

In additional to the ten NEG pumps surrounding the cathode electrode, each gun also has a small NEG pump [42] and a 40 liter/sec diode ion (DI) pump [43]. These latter pumps are mounted on ports of the chamber downstream of the gun anode electrode. This chamber also has ports for a quadrupole residual gas analyzer [44], an extractor gauge [45], an optical window and mirror assembly to allow illumination of the photocathode during activation, and sources of cesium and nitrogen trifluoride for cathode activation. The ten NEG pumps surrounding the cathode are insulated from the chamber walls and electrically connected in series. One end of the series string is electrically grounded, and the other connected to a standard high current vacuum feedthrough. The pumps are activated by Ohmic heating. Radiative heating from an isolated heater activates the additional small NEG pump. The DI pump primarily serves to pump chemically inert gases that may be present and are not pumped by the NEGs.

Each gun is mounted on a stainless steel table with a thermally insulating top. The thermal insulation is Micarta [46], closely packed in a covered stainless steel frame forming the table top. Five similarly constructed thermally insulating panels, with a few necessary cutouts, allow a complete oven to be quickly assembled around the gun. This enclosure forms the primary thermal insulation during bakeout. Bakeouts are accomplished by blowing heated air into the enclosure, using a 4 kW commercial heater system [47]. The use of flowing hot air and a suitable temperature ramp rate assures that the gun structure is heated uniformly without developing significant temperature differentials. The maximum bakeout temperature is typically 250 °C. The temperature is ramped up linearly over eight hours, held constant for thirty hours, and ramped down over eight hours. The gun DI pump has a side port that is connected, through a manual all-metal right-angle valve [48], to a similar pump outside the heated volume. This latter pump is the only one powered during bakeouts, and is valved out when bakeout is complete, after the gun pump is started.

Each polarized gun is isolated from the remainder of the injector by a 63 mm bore straight-through, all-metal pneumatic valve [49], located at the entrance to the chamber joining the two guns to the injector axis. A 1.3 m, 63.5 mm diameter NEG-coated tube joins the exit of the gun to this valve. During bakeout, this tube is heated by heating tapes. This tube has a captive solenoid lens that is bakeable to 250 °C.

The guns are vented to atmospheric pressure only to install new cathodes. Liquid nitrogen boiloff gas, pressurized to assure minimal back diffusion during cathode exchange, is used for venting. Great care is taken to minimize the time the system is at atmospheric pressure. Cathode exchanges require well under 1 min to complete. Rough pumping is done with a dry pumping system comprised of a molecular drag pump backed by a two-stage diaphragm pump [50]. Pump down from atmospheric pressure is rapid—the pressure typically falls below 10^{-8} mbar within 20 min after starting pumping. Prior to starting a bake, the cathode is exposed to cesium and photocurrent is detected. This step assures us that the cathode material is adequately clean before committing to a bakeout. During bakeout, the pressure rises no higher than about 5×10^{-8} mbar. It is clear during bakeout that the NEG pumps begin to activate at temperatures well below 250 °C, as the pressure begins to drop before the system reaches 200 °C, and continues to drop even as the temperature rises to 250 °C. We have demonstrated that we can exchange a photocathode wafer, complete a vacuum bakeout, and return the polarized gun to operation delivering beam in about 72 hours.

During the December of 1999 to January of 2000 shutdown, the vacuum conditions in each of the two nominally identical horizontal guns were studied. The extractor gauges and quadrupole residual gas analyzers (RGAs) on each gun were powered and left on to stabilize. Each gun was valved off from the injector vacuum during these measurements. After five days of continuous operation, the measured residual gas spectra were constant in time. The residual gas spectra, measured in two nominally identical electron guns that were not in vacuum communication, and with different but nominally identical RGAs, are given in Fig. 11. These spectra are essentially identical—an indication of the care used in the assembly and processing of these guns. The electron multiplier on each RGA was used, and no attempt to calibrate the electron multiplier for different mass gases was made. Each spectra shows only hydrogen, methane manifold, and a very small carbon monoxide signal. The prominence of the methane and carbon monoxide signals is not due to a large source of these gases, but rather to the exceptionally low hydrogen partial pressure, due to the large hydrogen pumping speed of the NEGs. The methane signal in each gun was observed

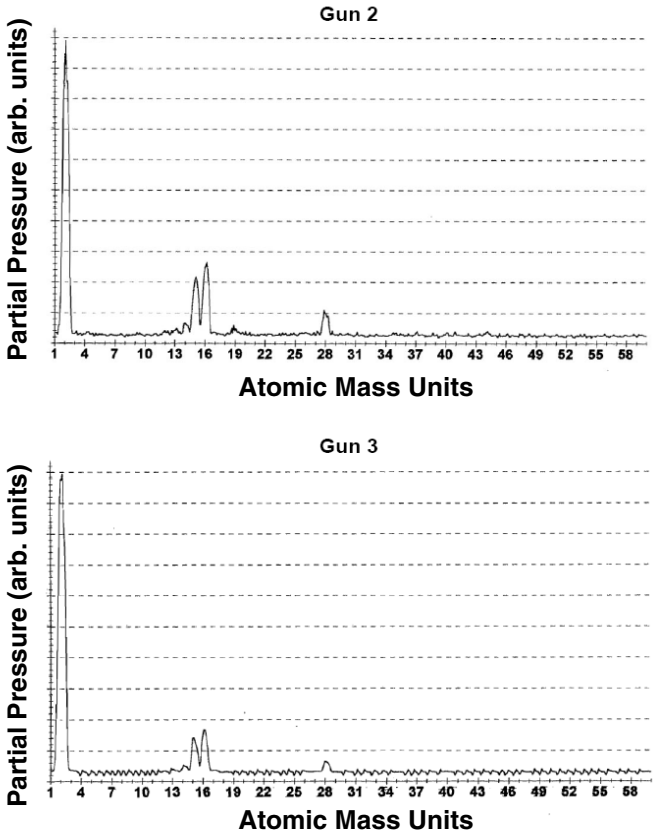

FIG. 11. Residual gas spectra for the nominally identical photoguns of the third polarized source. The spectra are virtually identical with hydrogen the dominant gas species. Trace amounts of methane (masses 12 through 16) and carbon monoxide are observed. The mass 19 peak is a result of electron stimulated desorption associated with our use of NF_3 for cathode activation. The labels Gun2 and Gun3 are historical designations, with Gun1 corresponding to the original CEBAF thermionic gun, now removed.

to decrease by ~20% when the valve isolating it from the main injector beam line was opened. Opening or closing this valve had no detectable effect on the hydrogen or carbon monoxide partial pressures. The small carbon monoxide peak is believed to arise from the filaments of the RGA and extractor gauge. The very small peak at mass 19 is an artifact of our use of NF_3 during photocathode activation, rather than indicating free fluorine atoms in the vacuum system.

It is difficult to determine the absolute pressure in the guns after bakeout, either during or without beam delivery. Both the RGA and the extractor gauge employ hot filaments as their electron sources. These are not operated during beam delivery. While the RGA is mounted with its filament and ionizer region distant from the chamber walls, this is not practical with the extractor gauge. It is reasonable to assume that, when the filaments are powered, these devices contribute to the gas load in the gun, and that they also provide a small pumping speed [51]. Knowing that the residual gas is predominantly hydrogen, we infer that the static total pressure in either gun is no greater than $\sim 10^{-11}$ mbar. We have developed an ion-pump power supply that permits the measurement of very tiny ion-pump currents [52]. These supplies are used on the gun chambers and beam line ion pumps through the injector. They allow us to readily observe very tiny beam scraping losses when they occur, and to demonstrate that there is no detectable pressure increase in the gun or along the beam line during normal beam delivery.

VII. PHOTOCATHODE PREPARATION PROCEDURES

Photocathode preparation involves a number of steps. Vendors provide strained GaAs in large (typically 50 or 76 mm diameter) wafers, from which suitably sized pieces are cut or cleaved. These pieces are then anodized to limit the active area of the final photocathode. Anodized samples are indium soldered to the molybdenum tip of a ''stalk,'' on which the cathodes are placed in the gun. Once mounted, the cathode material is cleaned by exposure to atomic hydrogen in a purpose-built system. Stalks with cleaned cathode material are transferred under dry nitrogen to the accelerator injector area, and the stalk mounted on the gun. Transferring the cathodes from the hydrogen cleaning chamber to the gun involves minimal exposure to air. Following vacuum bakeout as described above, the cathode is heated to ~550 °C to remove hydrogen from the bulk and loosely bound surface oxides. Cathodes are activated to negative electron affinity by successive applications of cesium and nitrogen trifluoride. Our procedures for these steps were developed over time, and are described in detail below.

We originally cut 15 mm diameter circular photocathode samples from larger commercial wafers using a diamond paste abrasive and a commercial semiconductor cutter. The large wafer was sandwiched between glass slides to protect its surface during cutting, using an acetone soluble adhesive. Considerable time was required to cut each sample and remove the adhesive. We now cleave 15 mm square samples, eliminating the use of adhesives and solvents, and requiring much less time. To cleave, a diamond tipped scribe is lightly dragged across the wafer. A slight pressure applied to the edge of the wafer then generates a clean break along the scribed line. The natural cleavage plane of GaAs is 110, perpendicular to the surface of our wafers, which are grown on 100 substrates. With care, surface contamination is not an issue during cleaving, as only the diamond tip touches the wafer surface.

To eliminate electron emission from large-radius regions of the photocathode, we anodize the samples to define an active photocathode area in the center of the sample. The anodic oxide, about 100 nm thick, is not removed during subsequent cleaning or heating, and does not support photoemission when the photocathode is activated [53]. We originally defined the active area of the photocathode by masking, using a drop of acetone soluble adhesive in the center of the sample as the mask, prior to the anodization. More recently, we use an O-ring sealed ''wand'' to hold the sample in the anodization bath. The sample is held on the wand with a soft vacuum inside the O-ring seal. This method eliminates the use of adhesives and solvents, reducing the chance of surface contamination in the active cathode area.

The cathode mounting stalk is a 66 cm long stainless steel tube with a molybdenum tip brazed to one end. A recess to accept the GaAs sample is machined into this tip, to a depth less than the thickness of the sample. The other end is welded into a standard 70 mm knife-edge flange. This flange is mounted on a translation mechanism on the gun, allowing the cathode to be moved into or extracted from its operating position in the Pierce cathode electrode. When the stalk reaches its operating position in the Pierce electrode, the translation mechanism smoothly separates from the mounting flange, and the stalk is held firmly in position by the atmospheric pressure load. A heater can be inserted into the stalk tube for heat cleaning or indium soldering the GaAs sample.

The GaAs wafers are held in the machined recess in the molybdenum tip by two means—indium soldering, and with a tantalum retaining ring. Originally, only the tantalum ring was used. Indium soldering is done by placing a 50 μm thick strip of indium foil in the molybdenum recess before adding the GaAs sample and the tantalum ring. The stalk tip is then briefly heated above the indium melting temperature. Indium soldering greatly improves the thermal contact between the GaAs and the molybdenum, and gives much better mechanical support to the GaAs wafer. When the cathode stalk is in its operating position in our guns, the edges of the GaAs wafer underneath the tantalum ring support the vacuum load on the stalk. Without me-

chanical support, this can easily crack the GaAs wafer, which may only be 300 μm thick. With the support provided by the indium solder, we have experienced no cracked wafers.

High quantum-efficiency negative electron-affinity photocathodes are prepared on GaAs by forming a dipole layer on the semiconductor surface. This dipole is formed by cesium and an oxidant, the latter typically either oxygen or fluorine. The dipole layer is nominally only one monolayer thick [54], with the dipole moment oriented to favor electron emission. For the highest quantum efficiency, it is necessary that the semiconductor surface be atomically clean prior to the formation of the dipole layer. Preparing an atomically clean semiconductor surface is a key step in the preparation of a high quantum yield photocathode.

For cleaning bulk GaAs, various wet chemical treatments were originally used. One of the most successful of these involved growing a ~100 nm thick anodic oxide layer on the GaAs surface. Immediately before installation of the cathode on the stalk, this oxide was removed with ammonium hydroxide, rinsed in methanol, and blown dry with liquid nitrogen boiloff gas. However, this method, like other wet chemical methods, removes a significant amount of material. As the thickness of the active layer of strained or multilayer GaAs wafers that provide high-polarization beam is only ~100 nm, methods that remove a large fraction of this thickness are unacceptable. Accordingly, we developed atomic hydrogen cleaning as a way to prepare atomically clean surfaces without removing cathode material [55]. Atomic hydrogen exposure has been shown to remove surface contaminants such as carbon and oxygen from a wide variety of semiconductors [56]. Furthermore, as noted in [56], hydrogen atoms passivate the dangling bonds at the GaAs surface, leaving a relatively inert surface.

We developed a small dedicated vacuum system for atomic hydrogen cleaning cathodes prior to their installation in the gun, shown in Fig. 12. Atomic hydrogen is produced by rf dissociation in a 2.5 cm Pyrex chamber, similar to the method used for some polarized hydrogen targets [57]. A 12 turn coil surrounds the Pyrex chamber and is contained in a conducting cylinder, forming an LC circuit resonant at ~100 MHz. The atomic hydrogen fraction is maximized when the hydrogen pressure in the chamber is ~20 mbar and the absorbed rf power is ~50 W. Atomic hydrogen exits the chamber through a ~1 mm diameter hole and is guided to the photocathode sample about 15 cm away by an aluminum tube. The aluminum gives a low hydrogen recombination rate. The photocathode sample is maintained at 300 °C during hydrogen cleaning [58]. A small turbomolecular pump and an ion pump remove the gas from the cleaning chamber. The pressure is maintained at $\sim 10^{-5}$ mbar during cleaning, limiting recombination by providing a long mean-free path for the atoms. Monte Carlo simulations predict that ~2.5% of the total atom flux reaches the photocathode. Under these conditions the atom flux at the cathode is estimated to be $\sim 10^{17}$ atoms/cm^2-sec, assuming 50% dissociation [59].

Both atomic hydrogen and deuterium have been used, with essentially identical results. The use of deuterium has the advantage that its signal is easy to distinguish from hydrogen with an RGA. We have measured the deuterium released by heating an atomic deuterium cleaned GaAs sample to determine the temperature-time product required to largely deplete the sample of deuterium. We have ob-

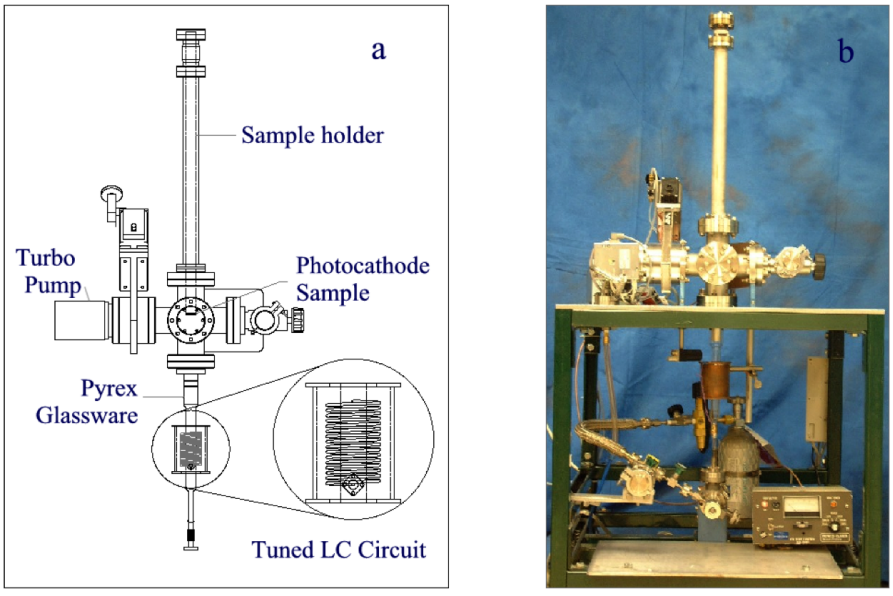

FIG. 12. (Color) The atomic hydrogen/deuterium source used to clean photocathodes prior to installation in the gun.

served that, while we can make very high quantum-efficiency photocathodes on bulk GaAs that has been cleaned with atomic hydrogen, the photocathode lifetime is short unless the hydrogen is subsequently removed by heat treatment. We presume the short lifetime is due to atomic hydrogen diffusing to the surface and degrading the dipole moment required to produce NEA.

Following the vacuum bakeout after installation of a new cathode wafer in the gun, the wafer is heated to high temperature before photocathode activation. This heating is done with a heater assembly inserted into the atmospheric pressure side of the stalk. The heater is a close-fitting molybdenum cylinder having a spiral gas passage machined in its outer surface. The cylinder contains a passage for gas exit, a cartridge heater, and a thermocouple passage. Dry nitrogen gas flows down the spiral channel of the heater and out the gas passage, providing good thermal contact between the heated cylinder and the tip area of the stalk. The thermocouple is maintained in firm contact with the back surface of the stalk with a spring. Heat cleaning is typically done for one hour at 675 °C, as measured by the thermocouple. The temperature at the surface of the GaAs is well below this temperature. This heat-cleaning step has empirically been shown to deplete the bulk cathode of hydrogen accumulated during atomic hydrogen cleaning.

While atomic hydrogen allowed us to reproducibly prepare high quantum-efficiency photocathode on both bulk GaAs and on various thin, high-polarization cathode materials, it has been shown more recently to be unnecessary on these latter cathode materials, if care is exercised to assure that the surface of these materials is never contaminated [60]. The high-polarization cathode materials are grown by epitaxial processes, and with proper handling have very clean surfaces. By cleaving, rather than cutting, and with the use of the vacuum wand during anodizing, we have found that we do not need any cleaning treatment at all to prepare high quantum-efficiency cathodes. Atomic hydrogen cleaning is likely to remain a useful technique for preparing cathodes on bulk materials, as might be used in a high average current, low-emittance photoemission gun, since the surfaces of these materials is likely contaminated during polishing.

Cathodes are activated on clean GaAs by alternating exposures to cesium and nitrogen trifluoride, beginning with cesium. During activation, the cathode is continuously illuminated with either white light or a suitable long wavelength diode laser. On the initial cesium exposure, the photoemission current reaches a maximum, and then decreases. We typically allow the photocurrent to decrease to about half of its maximum value before stopping the cesium exposure. On subsequent exposure to nitrogen trifluoride, the photocurrent rapidly increases to a new maximum, saturates, and then slowly decreases. Further exposure to cesium quickly produces a rapid decrease in the photocurrent. Again, we decrease the photocurrent to about half, followed by another nitrogen trifluoride exposure. This ''yo-yo'' process of forming the photocathode is widely used. In our guns, 12 to 15 Cs-NF_3 cycles are required to reach the final quantum efficiency. In the first polarized gun, we used an in-house built effusion cesium source as shown in Fig. 1, but changed to resistively heated commercial cesium dispensers [61] in subsequent guns. Two cesium dispensers wired in series, and high-purity nitrogen trifluoride introduced through an ultrahigh vacuum leak valve [62] provide the chemicals necessary for cathode activation.

VIII. CATHODE OPERATIONAL LIFETIME

There is nothing inherent in the photoemission process that degrades the quantum efficiency (QE) of a photocathode. Rather, the QE is degraded by physical processes such as chemical poisoning and ion back bombardment. Many different photocathodes have been operated stably for periods of many years in small volume, completely sealed vacuum environments. In these applications the cathodes deliver miniscule average currents and very small total charges. Achieving long photocathode operational lifetimes in a large-volume, actively pumped vacuum system, while delivering large average currents and large total charges, is the challenge for photoemission electron sources for accelerators.

The QE of NEA GaAs photocathodes is known to be rapidly degraded by exposure to certain chemically active gases, principally water, oxygen, and carbon dioxide, even in the absence of electron emission. In contrast, chemically inactive gases such as hydrogen, nitrogen, methane, argon, and carbon monoxide result in negligible degradation without emission [63–65]. The vacuum practices described above result in residual gas compositions in our guns that cause essentially no chemical degradation of the photocathode quantum efficiency. In one instance, we observed no measurable decrease in the QE of a freshly activated photocathode in the static vacuum of an unbiased and valved off gun over a period of nearly four months. If we make the conservative assumption that the calibration of our instruments for measuring optical power [66] and photoemission current [67] had changed such that we actually had an undetected 10% degradation of QE over this time, this would correspond to a 1/e dark lifetime of over 22 000 hours, or about two and a half years.

Field emission from the electrodes of the gun may release gases that result in cathode degradation, either from chemical poisoning or increased ion back bombardment during beam delivery. All electrode surfaces in our guns are carefully polished by hand with a series of finer and finer abrasives, finishing with 1 mm or smaller diamond paste. We have used both titanium and stainless steel as electrode materials. This polishing results in electrodes that show no measurable field emission at field strengths above those in our guns—about 6 MV/m. Although clean

titanium electrodes initially show no field emission, after exposure to cesium during only a few cathode activations they have unacceptably high field emission. Accordingly, we use only stainless steel for electrodes.

We have not measured the lifetime of a photocathode in a gun with high voltage applied but no photoemission. However, we observe no increase in the vacuum pressure when high voltage is applied to the gun, using the very sensitive pressure detection provided by the ion-pump power supplies we developed. Furthermore, our cathode operating lifetimes depend almost exclusively on the total integrated charge delivered, rather than the duration of time they have been operated at high voltage, implying that any effect due to high voltage alone is very small.

Thermal or chemical instability of NEA GaAs photocathodes has often been suggested as a possible source of QE degradation. This suggestion is based on the observation that application of cesium to a degraded photocathode can often restore the QE to very nearly its original value. However, Fischer *et al.* [68] have shown with careful x-ray photoelectron spectroscopy measurements that the cesium coverage of a GaAsP photocathode remains essentially constant during significant QE degradation and QE restoration by subsequent cesium exposure. Other measurements have shown that cesium is quite tightly bound to GaAs [69]. The fact that NEA GaAs photocathodes have shown widely differing lifetimes in different sources is further circumstantial evidence against cesium desorption as a significant source of QE degradation.

Ion back bombardment damage is a well-known phenomenon in thermionic electron guns, and is clearly important in photoemission guns. During the early days of operating GaAs photoemission guns, it was recognized that the QE degraded preferentially in the illuminated, and

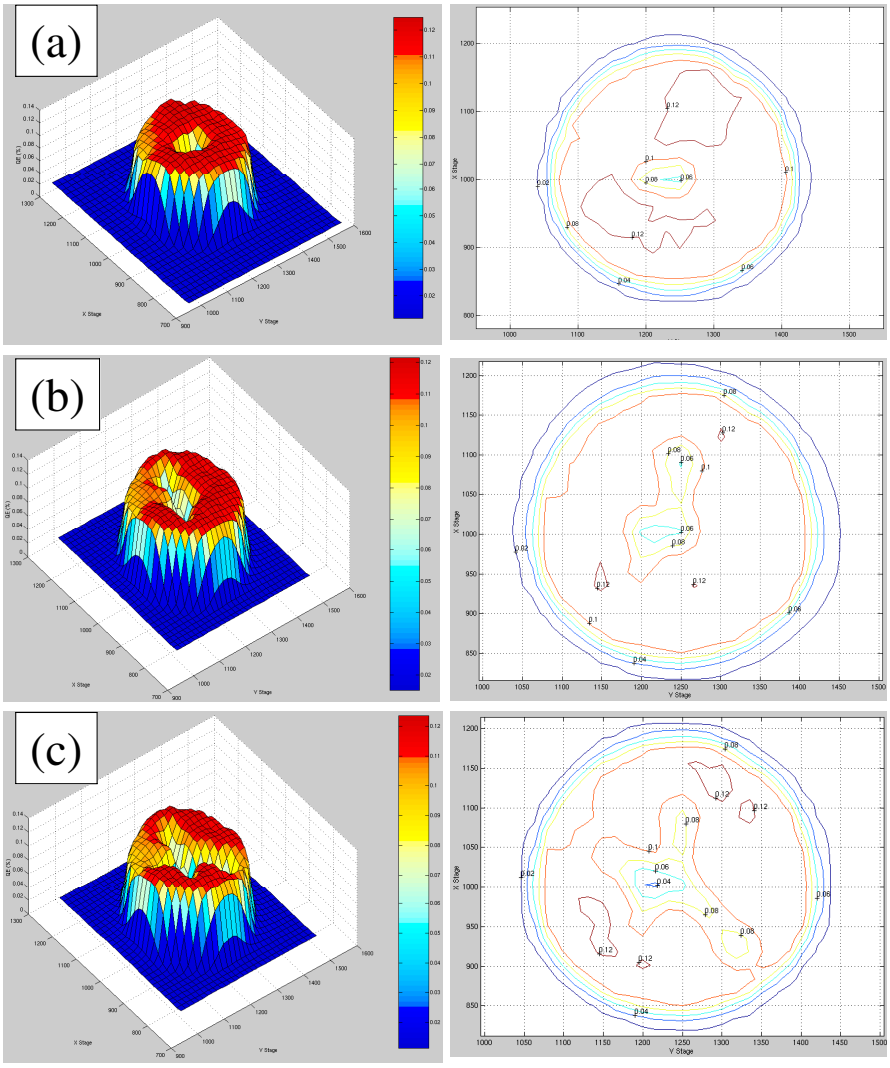

FIG. 13. (Color) QE scans of a photocathode obtained over many weeks of continuous operation. Beam was extracted from one location at a time, corresponding to each of the diagrams (a) through (c). The laser was moved to a new location on the photocathode after the QE had degraded sufficiently. The pattern of QE degradation indicates damage from ion back bombardment.

therefore emitting, area, which is a signature of ion back bombardment. Ion back bombardment as the origin of QE degradation was first convincingly demonstrated by the Mainz group [70]. This identification relied on the pattern of QE degradation produced by illuminating the cathode with a small laser spot displaced from the electrostatic axis of the gun. With a Pierce electrode providing focusing, the emitted electrons follow a trajectory toward the electrostatic axis, creating ions along their path. The ions are accelerated back to the cathode with very little transverse deflection. Thus, one expects to observe a pattern of QE degradation along a line from the illuminated spot toward the electrostatic center of the cathode, while the QE of the remaining unilluminated area is unchanged. This is exactly the QE degradation pattern reported by the Mainz group, and stands in contrast to the QE degradation expected from chemical poisoning or cesium desorption, which would be uniform over the cathode area. Although the probability of creating an ion decreases rapidly with electron energy, the QE damage an ion can cause at the photocathode rises with ion energy, and thus the QE damage region can extend radially inward from the illuminated spot for some distance.

The damage pattern observed in one of our guns is shown in Fig. 13. The QE degradation is shown following illumination at one, two, and three separated locations. Clearly, the QE of the unilluminated areas is unchanged, while the bands between the illuminated areas and the cathode electrostatic center are severely degraded. Note that the active area of the cathode is not centered at the electrostatic center of the cathode—a result of imperfect centering of the anodized ring we use to eliminate electrons from the large-radius areas of the cathode.

The residual gas spectrum in our guns is very largely composed of hydrogen. Hydrogen has a small, but finite sputter yield, and the QE damage may simply result from sputtering away the cesium-fluorine surface dipole that creates the NEA surface. Alternatively, the ions may physically damage the GaAs itself, hampering electron transport to the surface. We have observed that a cathode with a heavily degraded QE can be completely restored to its original QE by a cycle of heat cleaning and reactivation. This restoration cycle may be repeated many times without any apparent loss in initial QE. This supports the idea that the QE damage arises from sputtering of the cesium-fluorine activation layer rather than physical damage to the crystal, since the heat-cleaning cycle is unlikely to completely remove physical damage to the crystal. As the ion energy increases, the ions penetrate more deeply into the crystal, and ultimately the sputter yield decreases. Measurements of QE degradation as a function of cathode potential, done over a sufficiently large voltage range, may discriminate between sputtering and crystal damage as the primary mechanism of QE degradation. In any event, the only cure for QE degradation from ion back bombardment is a reduction of the total pressure in the cathode-anode gap region of the gun.

To characterize the ion back bombardment damage, we use the charge delivered per unit illuminated area that degrades the QE by a factor of 1/e. This is an imperfect characterization, since all the ions do not strike the illuminated area. However, by first illuminating areas close to the cathode electrostatic center, and moving the illuminated spots radially outward as the inner regions of the cathode are degraded, this charge density lifetime is a meaningful number for practical applications. With the vacuum we have achieved in our guns, we have measured charge density 1/e lifetimes of $\sim 2 \times 10^5$ C/cm^2. This corresponds to a 1/e QE degradation resulting from 200 C delivered from a ~ 350 μm diameter illuminated spot.

IX. LOAD-LOCKED GUN DEVELOPMENT

Prior to the excellent photocathode operational lifetimes achieved in the polarized guns reported here, polarized electron sources typically required a number of photocathode activations or recesiations to complete a physics experiment. Multiple cathode activations with the cathode in its operating location in the gun often led to degraded performance resulting from field emission from the cathode electrode structure. Some sources reported apparently irreversible cathode damage during beam delivery, requiring that the cathode wafer be replaced. Replacement of the photocathode requires a full vacuum bakeout followed by cathode cleaning and activation, involving considerable time during which no polarized beam delivery is possible. Some laboratories constructed a second polarized gun to allow cathode replacement in one gun while beam was delivered from the second. Other labs operated with unpolarized beam from a thermionic gun during cathode replacement. Load-locked polarized guns of various designs were developed at several laboratories in response to these problems [12–14,16,17,71]. In these designs, the cathode was activated outside of the electron gun structure and inserted into the cathode electrode of the gun through a load lock.

Load-locked gun designs offer several potential advantages. These include the possibility of achieving better ultimate vacuum since the gun chamber itself is never vented; reduced risk of field emission problems since the cathode electrode is never exposed to cesium; the possibility of having multiple cathodes prepared and stored in ultrahigh vacuum, ready for exchange with the operating cathode when necessary; and the ability to directly introduce cathode samples from outside the load-lock structure. These advantages are not obtained without corollary complications. The vacuum systems of these designs are considerably more complex than those of a simple photoemission gun. Load-locked guns must either have the load-lock apparatus at the cathode potential, or use a design that moves a cathode prepared at ground potential into the

high-voltage electrode structure. Reliably moving cathode samples between, and holding them in, the various devices and locations associated with cleaning, activating, and operating the cathode present many challenges. Attaching, moving, and releasing a mounted cathode brings the associated risk of dropping the cathode in an inconvenient location. Such lost samples can necessitate venting the gun or activation chambers to restore proper system function. Several laboratories operating load-locked guns have reported problems with dropped cathodes. Finally, heating and cooling thermally and mechanically isolated cathode assemblies in a complex vacuum system is far more difficult than when the cathode is attached in a mount with atmospheric pressure on one side.

We decided to design and build a load-locked gun, with the goals of extending the charge delivery lifetime of the cathode through improved vacuum; avoiding field emission problems by no longer activating the cathode in its high-voltage electrode; and reducing the time required to deliver beam from a new cathode by eliminating the need for a vacuum bakeout following cathode replacement. Our load-locked gun design [72] uses three chambers, as shown in Fig. 14: a loading/cleaning chamber; an activation chamber; and the gun chamber. The three chambers are separated from one another with all-metal gate valves [49]. Two orthogonal magnetic translation mechanisms move mounted cathodes between the loading/cleaning and activation chambers, and between the activation and gun chambers [73].

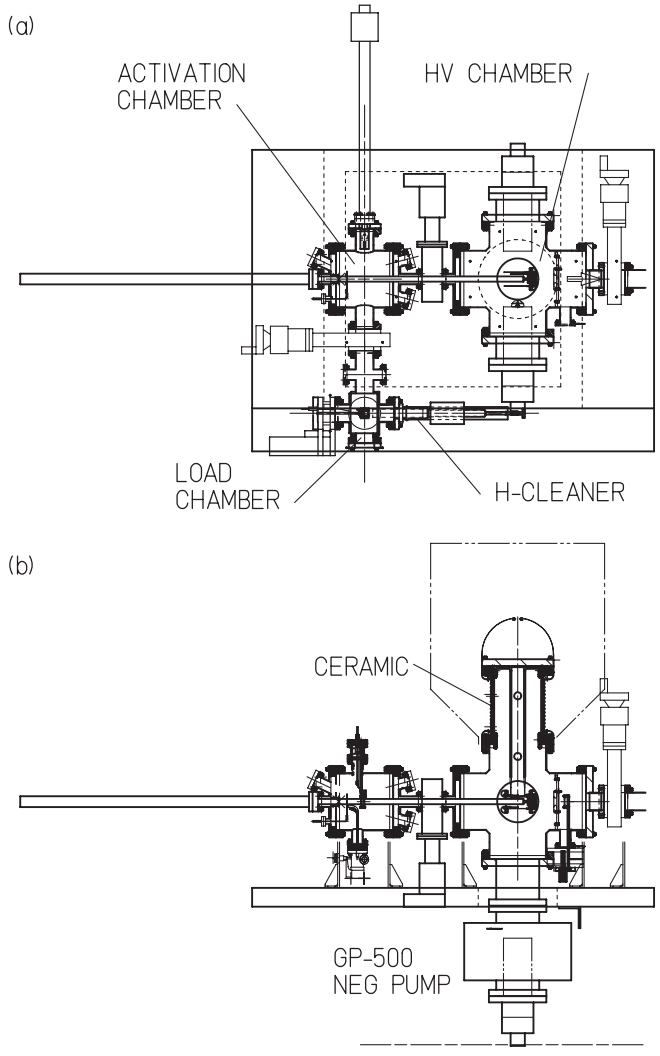

FIG. 14. The CEBAF load-locked gun: (a) top view; (b) side view.

The operating cathode assembly is mounted in a cylindrical cathode electrode structure, which in turn is supported from the high-voltage terminal of the ceramic insulator of the gun chamber—an arrangement that allows the loading and activation chambers to be at ground potential (this is not the only possible such arrangement). As with our other guns, a large amount of NEG pumping is incorporated in the gun chamber. Though not yet implemented, it would be straightforward to add a storage chamber for one or more additional cathodes in vacuum communication with the activation chamber. Both atomic hydrogen cleaning and heat cleaning of the cathode are possible in the loading/cleaning chamber. We have successfully taken GaAs wafers from the laboratory environment, cleaned and activated them, and moved them into the gun for beam operation in a total time of 12 hours [74]. Recently, this load-locked gun has been used to study cathode lifetimes at beam currents as high as 10 mA, using green light and bulk GaAs cathodes [75]. Realistically, the performance of the non-load-locked guns described in this article has reduced the need for a load-locked gun, and at the present time, this load-locked gun has not been installed at the injector.

X. CONCLUSIONS AND PROSPECTS FOR FUTURE POLARIZED SOURCE DEVELOPMENT

We have demonstrated a design for a high average current polarized electron source in which the operational lifetime of the photoemission cathode is limited almost exclusively by ion back bombardment. To date, we have reproducibly achieved, in each of two nominally identical guns, cathode 1/e dark lifetimes exceeding two years; cathode 1/e charge density lifetimes exceeding 2×10^5 C/cm^2; and total charge delivery from a single small illuminated spot exceeding 200 C. Unique laser systems were developed that assure that nearly 100% of the beam delivered from the photocathode reaches the experimental targets. Elimination of electrons originating from the large-radius regions of the photocathode was a very major advance. These large-radius electrons are apparently generated by photoemission from the recombination light produced in the cathode.

As ion back bombardment is the predominant lifetime-limiting phenomenon, further lifetime improvements will require reductions in the operating vacuum in the cathode-

anode gap region of the gun. The very large pumping speed obtained in these guns by the use of many NEG pumps leaves relatively little room for improvement from adding pumping speed. Instead, improvements in the ultimate pressure are likely to require reducing the gas source terms. This will likely require using more completely degassed wall materials, or perhaps extensive use of NEG coatings on the vacuum chamber walls. In parallel with reduced ultimate pressure, vacuum diagnostics improved over those available today will be necessary to quantitatively understand any gains made.

The observation that the only area of the photocathode to be degraded by ion back bombardment lies at and radially inside the illuminated area, and that a photocathode degraded by ion back bombardment can be fully restored by heat cleaning and reactivation, lead us to conclude that it may be better to concentrate on making a wisely selected pattern of illuminated spots on the cathode and a fast and efficient process for cleaning and reactivating the cathode without exposure of the cathode electrode surfaces to cesium, rather than investing in further load-locked gun development. Finally, although the developments described in this paper are directed toward generating polarized electron beams, many of them are well suited to application in photoemission electron sources to generate high average current, high brightness unpolarized beams.

ACKNOWLEDGMENTS

The work reported here was supported by the USDOE under Contract No. DE-AC05-84ER40150. During the course of this work, we received excellent support from many individuals. In particular, the superb mechanical design skills of Danny Machie are reflected in every detail of our polarized source designs. Jim Clark contributed greatly to many aspects of the mechanical construction of the system. Anthony Day and Kim Ryan helped develop and maintain the electronic control systems and computer interfaces through the many major polarized source changes. Our students Greg Thompson, Brian Archibald, Khaled El Amrawi, Keith Jones, Chris Hills, and Matt Inman helped with various technical details during their time with us. Reza Kazimi assisted with some of the beam commissioning work. The support and services provided by the Jefferson Laboratory machine shop were outstanding. More recent members of the polarized source group—Maud Baylac, Joe Grames, Marcy Stutzman, and Ken Surles-Law—have helped with some of the work described here, and have made additional and significant contributions that will be reported in future publications.

[1] C. W. Leemann *et al.*, Annu. Rev. Nucl. Part. Sci. **51**, 413 (2001).

[2] C. Reece *et al.*, *Proceedings of the 2001 Particle Accelerator Conference, Chicago, IL* (IEEE, New Jersey, 2001), p. 1186.

[3] C. K. Sinclair, Jefferson Laboratory Technical Note CEBAF-TN-96-032.

[4] J. M. Grames, Ph.D. thesis, University of Illinois at Urbana-Champaign, 2000.

[5] M. J. Alguard, J. E. Clendenin, R. D. Ehrlich, V. W. Hughes, J. S. Ladish, M. S. Lubell, K. P. Schuler, G. Baum, W. Raith, R. H. Miller, and W. Lysenko, Nucl. Instrum. Methods **163**, 29 (1979).

[6] W. von Drachenfels, U. T. Koch, Th. M. Muller, W. Paul, and H. R. Schaeffer, Nucl. Instrum. Methods **140**, 47 (1977).

[7] M. J. Alguard, J. E. Clendenin, P. S. Cooper, R. D. Ehrlich, V. W. Hughes, M. S. Lubell, G. Baum, and K. P. Schuler, Phys. Rev. A **16**, 209 (1977).

[8] L. A. Hodge, F. B. Dunning, and G. K. Walters, Rev. Sci. Instrum. **50**, 1 (1979).

[9] P. F. Wainwright, M. J. Alguard, G. Baum, and M. S. Lubell, Rev. Sci. Instrum. **49**, 571 (1978).

[10] D. T. Pierce, F. Meier, and P. Zurcher, Appl. Phys. Lett. **26**, 670 (1975).

[11] C. K. Sinclair, E. L. Garwin, R. H. Miller, and C. Y. Prescott, *A High Intensity Polarized Electron Source for the Stanford Linear Accelerator, in High Energy Physics with Polarized Beams and Targets, Argonne National Laboratory, 1976*, AIP Conference Proceedings 35, edited by M. L. Marshak (AIP, New York, 1976), p. 424.

[12] R. Alley, H. Aoyagi, J. Clendenin, J. Frisch, C. Garden, E. Hoyt, R. Kirby, L. Klaisner, A. Kulikov, R. Miller, G. Mulhollan, C. Prescott, P. Saez, D. Schultz, H. Tang, J. Turner, K. Witte, M. Woods, A. D. Yeremian, and M. Zolotorev, Nucl. Instrum. Methods Phys. Res., Sect. A **365**, 1 (1995).

[13] W. Hartmann, D. Conrath, W. Gasteyer, H. J. Gessinger, W. Heil, H. Kessler, L. Koch, E. Reichert, H. G. Andresen, T. Kettner, B. Wagner, J. Ahrens, J. Jethwa, and F. P. Schafer, Nucl. Instrum. Methods Phys. Res., Sect. A **286**, 1 (1990).

[14] K. Aulenbacher, Ch. Nachtigall, H. G. Andresen, J. Bermuth, Th. Dombo, P. Drescher, H. Euteneuer, H. Fischer, D. v. Harrach, P. Hartmann, J. Joffmann, P. Jennewein, K. H. Kaiser, S. Kobis, H. J. Kreidel, J. Langbein, M. Petri, S. Plutzer, E. Reichert, M. Schemies, H.-J. Schope, K. H. Steffens, M. Steigerwald, H. Trautner, and Th. Weis, Nucl. Instrum. Methods Phys. Res., Sect. A **391**, 498 (1997).

[15] G. D. Cates, V. W. Hughes, R. Michaels, H. R. Schaefer, T. J. Gay, M. S. Lubell, R. Wilson, G. W. Dodson, K. A. Dow, S. B. Kowalski, K. Isakovich, K. S. Kumar, M. E. Schulze, P. A. Souder, and D. H. Kim, Nucl. Instrum. Methods Phys. Res., Sect. A **278**, 293 (1989).

[16] M. J. J. van den Putte, C. W. De Jager, S. G. Konstantinov, V. Ya. Korchagin, F. B. Kroes, E. P. van Leeuwen, B. L. Militsyn, N. H. Papadakis, S. G. Popov, G. V. Serdobintsev, Yu. M. Shatunov, S. V. Shevelev, T. G. B. W. Sluijk, A. S. Terekhov, and Yu. F. Tokarev, *Seventh International Workshop on Polarized Gas Targets and Polarized Beams*, AIP Conf. Proc. No. 421 (AIP, New York, 1998), p. 260.

[17] W. Hillert *et al.*, AIP Conf. Proc. **570**, 961 (2001).
[18] B. M. Dunham, L. S. Cardman, and C. K. Sinclair, *Proceedings of the 1995 Particle Accelerator Conference, Dallas, TX* (IEEE, New Jersey, 1995), p. 1030.
[19] B. M. Dunham, Ph.D. thesis, University of Illinois at Urbana-Champaign, 1993.
[20] E. Reichert, as reported by C. K. Sinclair, *High-Energy Spin Physics, Eighth Annual Symposium*, AIP Conference Proceedings 187 (American Institute of Physics, Woodbury, NY, 1988), p. 1412.
[21] D. A. Engwall, B. M. Dunham, L. S. Cardman, D. P. Heddle, and C. K. Sinclair, Nucl. Instrum. Methods Phys. Res., Sect. A **324**, 409 (1993).
[22] K. Aulenbacher *et al.*, Proceedings of the 14th International Spin Physics Symposium, Osaka, Japan, 2000, p. 949.
[23] K. Halbach, Lawrence Livermore National Laboratory Technical Report No. UCRL-17436, 1967.
[24] J. M. Grames, C. K. Sinclair, J. Mitchell, E. Chudakov, H. Fenker, D. E. Higinbotham, M. Poelker, M. Steigerwald, M. Tiefenback, C. Cavata, S. Escoffier, F. Marie, T. Pussieux, P. Vernin, S. Danagoulian, V. Dharmawardane, R. Fatemi, K. Joo, M. Zeier, V. Gorbenko, R. Nasseripour, B. Raue, R. Sulieman, and B. Zihlmann, Phys. Rev. ST Accel. Beams **7**, 042802 (2004).
[25] NEG pump model WP-950-ST-707, from SAES Getters.
[26] Compact nested steering magnets, parts no. HRC 334 and no. HRC 335, from Haimson Research Corporation, Santa Clara, CA.
[27] T. Powers, in *Beam Instrumentation Workshop, Stanford, 1998*, AIP Conference Proceedings 451 (American Institute of Physics, Woodbury, NY, 1998), p. 256.
[28] K. A. Aniol *et al.*, Phys. Rev. Lett. **82**, 1096 (1999).
[29] T. Maruyama, E. L. Garwin, R. Prepost, and G. H. Zapalac, Phys. Rev. B **46**, 4261 (1992). This material can be purchased from Bandwidth Semiconductor, LLC, 25 Sagamore Park Drive, Hudson, NH 03051.
[30] T. Maruyama, D.-A. Luh, A. Brachmann, J. E. Clendenin, E. L. Garwin, S. Harvey, J. Jiang, R. E. Kirby, A. M. Moy, R. Prepost, and C. Y. Prescott, Appl. Phys. Lett. **85**, 2640 (2004). Material can be purchased from SVT associates, Inc., 7620 Executive Drive, Eden Prairie, MN 55344.
[31] T. Hiatt, Jefferson Laboratory Technical Note TN-06-049.
[32] C. Benvenuti, P. Chiggiato, F. Cicoira, and Y. L'Aminot, J. Vac. Sci. Technol. A **16**, 148 (1998).
[33] C. Benvenuti, P. Chiggiato, F. Cicoira, and Y. L'Aminot, Vacuum **50**, 57 (1998).
[34] J. J. Welch and C. K. Sinclair, SLAC Report 303, Stanford, CA, p. 87.
[35] M. Poelker, Appl. Phys. Lett. **67**, 2762 (1995).
[36] D.-X. Wang, G. A. Krafft, and R. Abbott, Jefferson Laboratory Technical Note TN-94-054.
[37] B. Dunham, Jefferson Laboratory Technical Note TN-96-042.
[38] A. V. Aleksandrov *et al.*, Phys. Rev. E **51**, 1449 (1995).
[39] P. Hartmann *et al.*, Proceedings of the Workshop on Polarized Electrons and Low-Energy Polarimeters, Amsterdam, 1996. Published in the *Proceedings of the 12th International Symposium on High Energy Spin Physics (SPIN96)*, edited by C. W. de Jager *et al.* (World Scientific Publishing Co., Singapore, 1996); also P. Hartmann *et al.*, Nucl. Instrum. Methods Phys. Res., Sect. A **379**, 15 (1996).
[40] Optical autocorrelator model FR-103XL from Femtochrome Research Inc., 2123 4th Street, Berkeley, CA 94710.
[41] C. Hovater and M. Poelker, Nucl. Instrum. Methods Phys. Res., Sect. A **418**, 280 (1998); U.S. Patent No. 6483858; M. Poelker and J. Hansknecht, IEEE Particle Accelerator Conference, Chicago, IL, 2001.
[42] GP100 Sorb-AC cartridge pump on $4.5''$ knife-edge flange, with ST 707 material from SAES Getters.
[43] DI pumps purchased from Perkin Elmer, now Gamma Vacuum, 2915 13rd Street West, Shakopee, MN 55379. Perkin Elmer model 204-3000, 30 L/s nominal pump speed. Gamma Vacuum model Titan DI-40s-4D, 35 L/s nominal pump speed.
[44] Residual gas analyzer model RGA200 manufactured by Stanford Research Systems, 1290-D Reamwood Avenue, Sunnyvale, CA 94089.
[45] Ionivac IM 520 extractor gauge manufactured by Leybold Vacuum GmbH, Bonner Strasse 498, D-50968, Koln, Germany.
[46] Compressed Fibrefrax sheets, $2''$ thick, $2' \times 4'$ panels, Part No. 739781100 Thermal Products Company, Inc. 4520 S. Berkeley Lake Road, Norcross, GA 30071-1639.
[47] Leister Type 5000 hot air tool, 4 kW at 220VAC, in combination with Leister ''Silence'' air blower.
[48] Bakeable right-angle, all-metal valve from Vacuum Generators, Model VZCR40R, purchased from Kurt J. Lesker Company, P.O. Box 10, 1925 Route 51, Clairton, PA 15025-2700.
[49] All-metal gate valve with pneumatic actuator bakeable to 300 C, Series 48, from VAT Inc., 500 West Cummings Park, Suites 5450-5650, Woburn, MA 01801. Manually actuated gate valves of this design were used to isolate chambers of the load-locked gun.
[50] Oil-free roughing pump, Drytel 100, consisting of a molecular drag pump (model 5030) backed by a diaphragm pump (model 85501) from Alcatel Vacuum Products (now Adixen), 67 Sharp Street, Hingham, MA 02043.
[51] P. A. Redhead, J. Vac. Sci. Technol. A **12**, 904 (1994); P. A. Redhead, Vacuum **53**, 137 (1999).
[52] Ultrahigh vacuum ion-pump power supply with pump current resolution <1 nA. Model EOS-902, from Eye On Science LLC, 527 Lakeshead Dr., Williamsburg, VA 23185.
[53] P. M. Rutt and A. R. Day, Jefferson Laboratory Technical Note TN-01-030; M. Stutzman, Jefferson Laboratory Technical Note TN-05-083. A description of the basic anodizing procedure can be found in B. M. Dunham and C. K. Sinclair, NPL Polarized Source Group Technical Note No. 90-3, University of Illinois, Urbana/Champaign and in B. Schwartz *et al.*, J. Electrochem. Soc. **123**, 1089 (1976).
[54] V. L. Alperovich, A. G. Paulish, H. E. Scheibler, and A. S. Terekhov, Appl. Phys. Lett. **66**, 2122 (1995).
[55] C. K, Sinclair, B. M. Poelker, and J. S. Price, in *Proceedings of the 1997 Particle Accelerator Conference, Vancouver, BC* (IEEE, Piscatasay, NJ, 1997), p. 2864.
[56] Y. Okada and J. S. Harris, J. Vac. Sci. Technol. B **14**, 1725 (1996).

[57] M. Poelker, K. P. Coulter, R. J. Holt, C. E. Jones, R. S. Kowalczyk, L. Young, B. Zeidman, and D. K. Toporkov, Nucl. Instrum. Methods Phys. Res., Sect. A **364**, 58 (1995).

[58] E. Petit and F. Houzay, J. Vac. Sci. Technol. B **12**, 547 (1994).

[59] M. Poelker, K. P. Coulter, R. J. Holt, C. E. Jones, R. S. Kowalczyk, L. Young, B. Zeidman and D. K. Toporkov, Phys. Rev. A **50**, 2450 (1994); and C. Baumgartner *et al.*, Nucl. Instrum. Methods Phys. Res., Sect. A **508**, 268 (2003).

[60] M. Baylac, P. Adderley, J. Brittian, J. Clark, T. Day, J. Grames, J. Hansknecht, M. Poelker, M. Stutzman, A. T. Wu, and A. S. Terekhov, Phys. Rev. ST Accel. Beams **8**, 123501 (2005).

[61] Cesium dispenser from SAES Getters, Part No. Cs/NF/5.4/25/FT10+10.

[62] UHV gas dosing valve, Balzers UDV 035 from Pfeiffer Vacuum, 24 Trafalgar Square, Nashua, NH 03063.

[63] C. K. Sinclair, in *Advanced Accelerator Concepts*, edited by F. E. Mills, AIP Conference Proceedings No. 156 (American Institute of Physics, Woodbury, NY, 1987), p. 298.

[64] T. Wada, T. Nitta, T. Nomura, M. Miyao, and M. Hagino, Jpn. J. Appl. Phys. **29**, 2087 (1990).

[65] D. Durek, R. Hoffmann, T. Reichelt, and M. Westermann, in *Proceedings of the 12th International Symposium on High Energy Spin Physics (SPIN96)*, edited by C. W. de Jager *et al.* (World Scientific Publishing Co., Singapore, 1997), p. 677.

[66] Optical power meter Model 1830-C with 818-SL/CM detector head and calibration module from Newport Corporation, 1791 Deere Avenue, Irvine, CA 92606.

[67] Autoranging picoammeter, model 485/4853 from Keithley Instruments, Inc, 28775 Aurora Road, Cleveland, Ohio 44139.

[68] H. Fischer, P. Drescher, and E. Reichert, SLAC 432-Rev., SLAC, Stanford, CA, 1994, p. 249.

[69] B. Goldstein and D. Szostak, Appl. Phys. Lett. **26**, 111 (1975).

[70] K. Aulenbacher, SLAC 432-Rev., SLAC, Stanford, CA, 1994, p. 1.

[71] M. Breidenbach, M. Foss, J. Hodgson, A. Kulikov, A. Odian, G. Putallaz, H. Rogers, R. Schindler, K. Skarpaas, and M. Zolotorev, Nucl. Instrum. Methods Phys. Res., Sect. A **350**, 1 (1994).

[72] W. Schneider *et al.*, in *Proceedings of the 1999 Particle Accelerator Conference, New York* (IEEE, Piscataway, NJ, 1999), p. 1991.

[73] Ultrahigh vacuum sample manipulators from Transfer Engineering and Manufacturing, 47697 Westinghouse Drive, Suite 100, Fremont, CA 94539.

[74] M. Stutzman *et al.*, in Proceedings of the Workshop on Polarized Electron Sources and Polarimeters, Danvers, Massachussetts; published with the Proceedings of the 15th International Spin Physics Symposium (SPIN 2002), p. 1078.

[75] M. Poelker *et al.*, in the Proceedings of the 11th International Workshop on Polarized Sources and Targets, Tokyo, Japan (to be published); and J. Grames *et al.*, in the Proceedings of the 17th International Spin Physics Symposium, Kyoto, Japan (to be published).